Defense Nuclear Agency
Alexandria, VA 22310-3398

DNA-TR-94-49

High Power Microwave Source Development

James N. Benford, et al.
Physics International Co.
P.O. Box 5010
San Leandro, CA 94577-0599

Gabriel Miller
Seth Potter
New York University
Barney Building
26-36 Stuyvesant Street
New York, NY 10003

May 1995

Technical Report

CONTRACT No. DNA 001-89-C-0032

Destroy this report when it is no longer needed. Do not return to sender.

PLEASE NOTIFY THE DEFENSE NUCLEAR AGENCY, ATTN: CSTI, 6801 TELEGRAPH ROAD, ALEXANDRIA, VA 22310-3398, IF YOUR ADDRESS IS INCORRECT, IF YOU WISH IT DELETED FROM THE DISTRIBUTION LIST, OR IF THE ADDRESSEE IS NO LONGER EMPLOYED BY YOUR ORGANIZATION.

DNA PRINTING PLANT

DISTRIBUTION LIST UPDATE

This mailer is provided to enable DNA to maintain current distribution lists for reports. (We would appreciate your providing the requested information.)

☐ Add the individual listed to your distribution list.

☐ Delete the cited organization/individual.

☐ Change of address.

NOTE:
Please return the mailing label from the document so that any additions, changes, corrections or deletions can be made easily. For distribution cancellation or more information call DNA/IMAS (703) 325-1036.

NAME: _____

ORGANIZATION: _____

OLD ADDRESS	CURRENT ADDRESS
_____	_____
_____	_____
_____	_____

TELEPHONE NUMBER: ( ) _____

DNA PUBLICATION NUMBER/TITLE	CHANGES/DELETIONS/ADDITIONS, etc.) *(Attach Sheet if more Space is Required)*
_____	_____
_____	_____
_____	_____

DNA OR OTHER GOVERNMENT CONTRACT NUMBER: _____

CERTIFICATION OF NEED-TO-KNOW BY GOVERNMENT SPONSOR (if other than DNA):

SPONSORING ORGANIZATION: _____

CONTRACTING OFFICER OR REPRESENTATIVE: _____

SIGNATURE: _____

CUT HERE AND RETURN

REPORT DOCUMENTATION PAGE

Form Approved OMB No. 0704-0188

1. AGENCY USE ONLY (Leave blank)	2. REPORT DATE	3. REPORT TYPE AND DATES COVERED
	950501	Technical 890602 – 931231

4. TITLE AND SUBTITLE

High Power Microwave Source Development

5. FUNDING NUMBERS

C - DNA 001-89-C-0032
PE - 4662D
PR - BA RL
TA - BA RA
WU - DH890032

6. AUTHOR(S)

James N. Benford, Steve Ashby, Richard R. Smith, Normal Aiello, Nicholas J. Cooksey, David V. Drury, Peter Sincerny, Lance Thompson, Leland Smith, Jerrold S. Levine, Bruce Harteneck (Physics International Co.); Gabriel Miller and Seth Potter (New York University).

7. PERFORMING ORGANIZATION NAME(S) AND ADDRESS(ES)

Physics International Co.
P.O. Box 5010
San Leandro, CA 94577-0599

New York University
Barney Building
26-36 Stuyvesant Street
New York, NY 10003

8. PERFORMING ORGANIZATION REPORT NUMBER

PIFR-4129-D

9. SPONSORING/MONITORING AGENCY NAME(S) AND ADDRESS(ES)

Defense Nuclear Agency
6801 Telegraph Road
Alexandria, VA 22310-3398
RAST/Manriquez

10. SPONSORING/MONITORING AGENCY REPORT NUMBER

DNA-TR-94-49

11. SUPPLEMENTARY NOTES

This work was sponsored by the Defense Nuclear Agency under RDT&E RMC Codes B2637D BA BA 00011 RAEV 3300A 25904D and B4693C RL RA 00010 RAEV 3300A 25904D.

12a. DISTRIBUTION/AVAILABILITY STATEMENT

Approved for public release; distribution is unlimited.

12b. DISTRIBUTION CODE

13. ABSTRACT *(Maximum 200 words)*

The requirements of this project have been to:

1) improve and expand the sources available in the facility for testing purposes, and
2) perform specific tasks under direction of DNA about the applications of HPM. In the previous program many such tasks were undertaken. In this project the HPM application was power beaming.

The requirements of this program were met in the following way:

1) We demonstrated that a compact linear induction accelerator can drive HPM sources at repetition rates in excess of 100 HZ at peak microwave powers of a GW. This was done for the relativistic magnetron. Since the conclusion of this contract such specifications have also been demonstrated for the relativistic klystron under BMDO funding.
2) We demonstrated an L-band relativistic magnetron, the first of its kind. This device has been used both on our single pulse machines, CAMEL and CAMEL X, and the repetitive system CLIA.
3) We demonstrated that phase locking of sources together in large numbers is a feasible technology and showed the generation of multigigawatt S-brand radiation in an array of relativistic magnetrons.

14. SUBJECT TERMS

Repetitive
Phase Locking
Relativistic Magnetrons
HPM Sources
Relativistic Klystrons

15. NUMBER OF PAGES

70

16. PRICE CODE

17. SECURITY CLASSIFICATION OF REPORT	18. SECURITY CLASSIFICATION OF THIS PAGE	19. SECURITY CLASSIFICATION OF ABSTRACT	20. LIMITATION OF ABSTRACT
UNCLASSIFIED	UNCLASSIFIED	UNCLASSIFIED	SAR

NSN 7540-280-5500

Standard Form 298 (Rev.2-89)
Prescribed by ANSI Sta. 239-18
298-102

CLASSIFIED BY:

N/A since Unclassified.

DECLASSIFY ON:
N/A since Unclassified.

13. ABSTRACT (continued)

4) We partially developed a relativistic klystron amplifier with a broad range of tunability or frequency agility. Frequency agility is likely to be a feature of high power microwave weapons which could threaten U.S. equipment.

The lessons learned in this project are that:

1) HPM sources can be operated at high repetition rates if suitable design principles are used. These principles relate to the use of clean surfaces and good vacuum technique.
2) Greater power is available at lower frequencies. Device scaling indicates this and it has now been verified at high powers.
3) Phase locking of oscillators is a practical technique. Phase locking can be used to generate powers of ~10 GW and may even extrapolate to 100 GW levels.
4) Frequency agility is practical at high power.

CONVERSION TABLE

Conversion factors for U.S. Customary to metric (SI) units of measurement.

MULTIPLY → / ← TO GET	BY → / ← BY	TO GET / DIVIDE
angstrom	1.000 000 X E -10	meters (m)
atmosphere (normal)	1.013 25 X E +2	kilo pascal (kPa)
bar	1.000 000 X E +2	kilo pascal (kPa)
barn	1.000 000 X E -28	meter^2 (m^2)
British thermal unit (thermochemical)	1.054 350 X E +3	joule (J)
calorie (thermochemical)	4.184 000	joule (J)
cal (thermochemical/cm^2)	4.184 000 X E -2	mega joule/m^2 (MJ/m^2)
curie	3.700 000 X E +1	* giga becquerel (GBq)
degree (angle)	1.745 329 X E -2	radian (rad)
degree Fahrenheit	t_k = (t °f + 459.67)/1.8	degree kelvin (K)
electron volt	1.602 19 X E -19	joule (J)
erg	1.000 000 X E -7	joule (J)
erg/second	1.000 000 X E -7	watt (W)
foot	3.048 000 X E -1	meter (m)
foot-pound-force	1.355 818	joule (J)
gallon (U.S. liquid)	3.785 412 X E -3	meter^3 (m^3)
inch	2.540 000 X E -2	meter (m)
jerk	1.000 000 X E +9	joule (J)
joule/kilogram (J/kg) radiation dose absorbed	1.000 000	Gray (Gy)
kilotons	4.183	terajoules
kip (1000 lbf)	4.448 222 X E +3	newton (N)
kip/inch^2 (ksi)	6.894 757 X E +3	kilo pascal (kPa)
ktap	1.000 000 X E +2	newton-second/m^2 (N-s/m^2)
micron	1.000 000 X E -6	meter (m)
mil	2.540 000 X E -5	meter (m)
mile (international)	1.609 344 X E +3	meter (m)
ounce	2.834 952 X E -2	kilogram (kg)
pound-force (lbs avoirdupois)	4.448 222	newton (N)
pound-force inch	1.129 848 X E -1	newton-meter (N•m)
pound-force/inch	1.751 2688 X E +2	newton/meter (N/m)
pound-force/foot^2	4.788 026 X E -2	kilo pascal (kPa)
pound-force/inch^2 (psi)	6.894 757	kilo pascal (kPa)
pound-mass (lbm avoirdupois)	4.535 924 X E -1	kilogram (kg)
pound-mass-foot^2 (moment of inertia)	4.214 011 X E -2	kilogram-meter^2 (kg•m^2)
pound-mass/foot^3	1.601 846 X E +1	kilogram/meter^3 (kg/m^3)
rad (radiation dose absorbed)	1.000 000 X E -2	** Gray (Gy)
roentgen	2.579 760 X E -4	coulomb/kilogram (C/kg)
shake	1.000 000 X E -8	second (s)
slug	1.459 390 X E +1	kilogram (kg)
torr (mm Hg, 0° C)	1.333 22 X E -1	kilo pascal (kPa)

*The becquerel (Bq) is the SI unit of radioactivity; 1 Bq = 1 event/s.
**The Gray (GY) is the SI unit of absorbed radiation.

TABLE OF CONTENTS

Section		Page
	CONVERSION TABLE	iii
	FIGURES	v
1	INTRODUCTION	1
2	PULSED POWER DEVELOPMENT	4
3	SOURCE DEVELOPMENT	7
4	FACILITY OPERATIONS AND UPGRADES	11
Appendix		
A	PULSED POWER PAPER	A-1
B	SOURCE DEVELOPMENT PAPERS	B-1
C	POWER BEAMING REPORT	C-1

FIGURES

Figure		Page
2-1	Pulse-forming lines and induction of cores of CLIA	5
3-1	Repetitive L-band magnetron on CLIA	8
3-2	Multiple-magnetron phase-locking machine with four magnetrons	9
3-3	Seven-magnetron module in central connection geometry	10
4-1	Configuration of the S-band broad-bandwidth relativistic klystron	12
4-2	S-band relativistic klystron under assembly	13
4-3	Five shot overlay at ~ 1 pps	15

SECTION 1

INTRODUCTION

High power microwave (HPM) technology is being developed in the U.S. for a variety of both military and nonmilitary applications. In the military arena, the tactical applications for HPM weapons have grown to dominate the national effort after an initial SDI based strategic program in the middle 1980's. There is evidence of widespread interest abroad in HPM, which may result in HPM threats to U.S. equipment.

Consequently, a program has been underway for the last ten years which has investigated many aspects of HPM technology. It is sponsored by DNA and located at Physics International Company (PI). In a previous report, (DNA TR-89-31-V1, *High Power Microwave Source and Facility Development*) initial efforts in this program were described. An HPM testing facility was constructed so that the effects of HPM on military electronics could be assessed. This facility has been open for testing activities since mid 1985. A variety of systems and electronic packages have been tested in high power environments. The facility was than expanded to include lower power capabilities and simulation of a variety of sophisticated defeat mechanisms. Source development has continued in order to broaden the capability of the DNA/BMDO facility.

The requirements of this project have been to:

1) improve and expand the sources available in the facility for testing purposes, and

2) perform specific tasks under direction of DNA about the applications of HPM. In the previous program many such tasks were undertaken. In this project the HPM application was power beaming.

The requirements of this program were met by

1) Demonstrating that a compact linear induction accelerator can drive HPM sources at repetition rates in excess of 100 Hz at peak microwave powers of a GW. This was done for the relativistic magnetron. Since the conclusion of this contract such specifications have also been demonstrated for the relativistic klystron under BMDO funding.

2) Demonstrating an L-band relativistic magnetron, the first of its kind. This device has been used both on our single pulse machines, CAMEL and CAMEL X, and the repetitive system CLIA.

3) Demonstrating that phase locking of sources together in large numbers is a feasible technology and showed the generation of multigigawatt S-band radiation in an array of relativistic magnetrons.

4) Partially developing a relativistic klystron amplifier with a broad range of tunability or frequency agility. Frequency agility is likely to be a feature of high power microwave weapons which could threaten U.S. equipment.

The lessons learned in this project are that:

1) HPM sources can be operated at high repetition rates if suitable design principles are used. These principles relate to the use of clean surfaces and good vacuum technique.

2) Greater power is available at lower frequencies. Device scaling indicates this and it has now been verified at high powers.

3) Phase locking of oscillators is a practical technique. Phase locking can be used to generate powers of ~ 10 GW and may even extrapolate to 100-GW levels.

4) Frequency agility is practical at high power.

In order to make the substantial amount of information in this report readily accessible, introductory sections are brief; they are supported by appendices which describe many aspects of the work in considerable detail.

Section 2 describes the development of a repetitive pulse power system for driving HPM sources. The system is called Compact Linear Induction Accelerator (CLIA) and is described in detail in Appendix A.

Section 3 describes the development of relativistic magnetrons to lower frequency and the phase-locking of an array of relativistic magnetron. Appendix B contains papers detailing these developments.

Section 4 describes the development of a relativistic klystron amplifier with frequency tunability/agility. Initial use was in tests of the Pershing II GIEU system.

The applications task executed under this program was a subcontract to New York University, Department of Applied Science. This task was a study of earth-to-satellite microwave power transmission to provide recharging power to an orbiting SDI platform. The system analysis is contained in Appendix C.

SECTION 2

PULSED POWER DEVELOPMENT

The generation of microwaves at high power has progressed largely with single shot devices. Applications, however, require repetitive operation at substantial repetition rates, implying high average power.

An attractive pulse power system for high repetition rate HPM is the hard-core linear-induction accelerator (LIA), where "hard-core" refers to a central cathode shank, not an electron beam. The repetitive operation advantage of the LIA stems from all pulse compression being done at moderate voltages. It uses the accelerator structure to add parallel voltage pulses into a single high voltage output. In addition, systems using magnetic pulse compression for switching have inherently long lifetime and eliminate the erosion problems of spark gaps.

This system is compact, which is an advantage for any application. The basic reason for the compactness is that the voltage from individual sections is added up in vacuum so that the peak voltage appears only on the load.

To pursue this line of development, under this program we have built a compact LIA system (CLIA) consisting of a ten-cell accelerator driven by ten magnetically switched water-insulated PFLs. The induction cells and PFLs of CLIA are shown in Figure 2-1. These are charged in turn by a single two-stage magnetic compression unit, which in turn is driven by a thyratron-switched intermediate energy store unit and command resonant charge unit.

The CLIA system was developed to achieve the specifications shown in Table 2-1. These specifications have been achieved. The facility is now used for a variety of HPM source development and testing functions. Appendix A contains a brief description of the CLIA system in its initial 60-ns manifestation. The pulse duration was later extended to 100 ns. This extension capability was included in the original design. Appendix B contains two papers describing CLIA operation with magnetrons and klystrons.

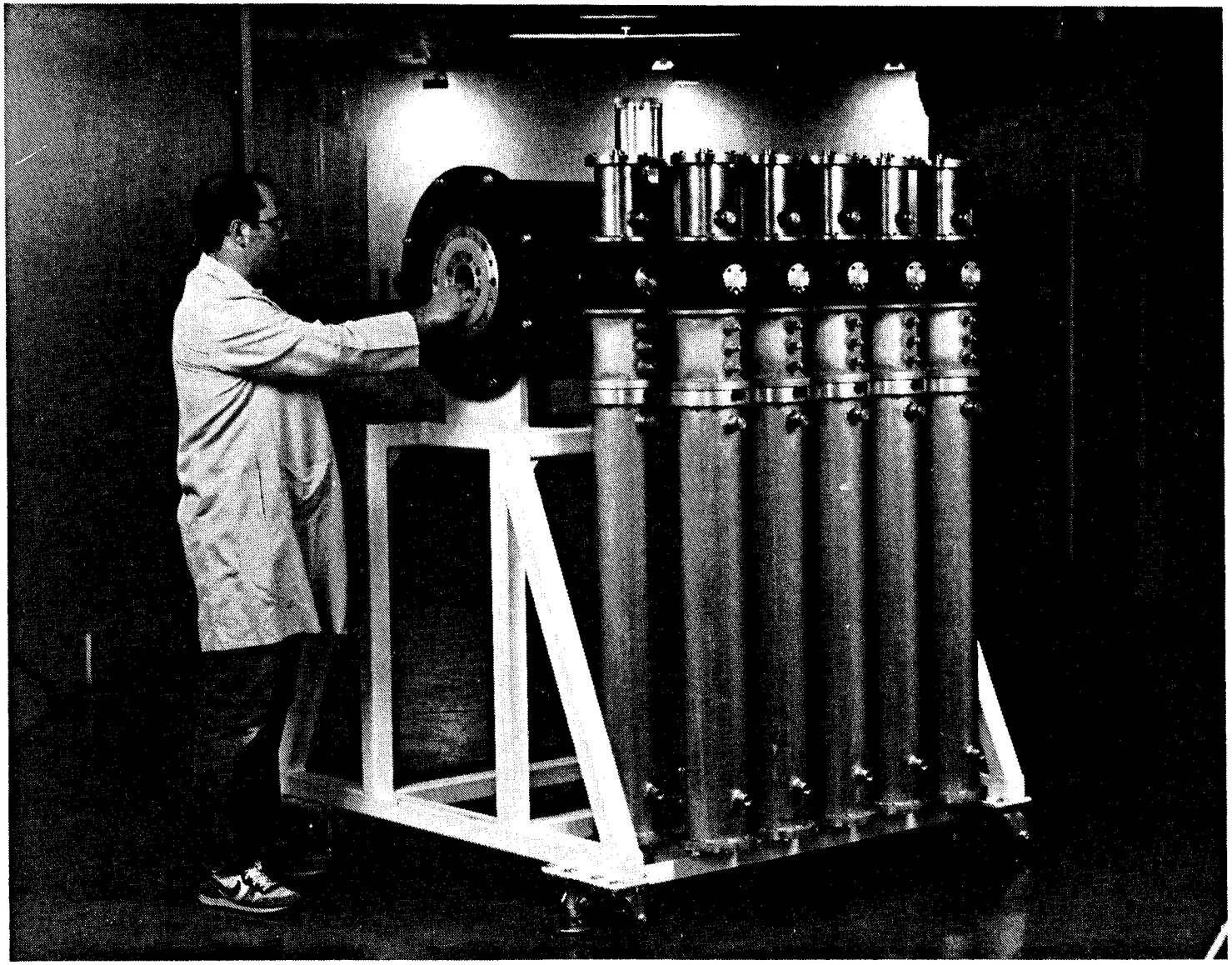

Figure 2-1. Pulse forming lines and induction cores of CLIA.

Table 2-1. CLIA parameters.

Output Voltage	750 kV
Output Current	10 kA
Impedance	75 Ω
Pulse Duration	100 ns (upgraded from initial 60 ns operation)
Beam Peak Power	7.5 GW
Energy per Pulse	750 joules
Average Power	150 kW
Repetition Rate	200 pps

SECTION 3

SOURCE DEVELOPMENT

Source development activities have proceeded along two completely different directions. The first was to use CLIA, which is described in Section 2, to operate high power sources repetitively at high repetition rates. The first source to be so developed was the L-band relativistic magnetron, shown in Figure 3-1. The initial operation of the magnetron ran into some difficulties with "dropouts" due to breakdown inside the resonator. The fundamental cause was surface contamination. Secondary causes were virtual leaks and outgassing from plastic anodized surfaces. After eliminating these contamination sources, we were able to operate the magnetron at 1 GW peak power at a repetition rate of 100 Hz and 0.7 GW at 200 Hz, thereby achieving average powers of ~6 kW. We also demonstrated a 600 MW, 1,000 Hz burst of five shots. These experiments are described in Appendix B.

The second line of development was the phase locking of oscillators together to produce much higher powers than are available in a single source. We conducted an experiment with up to seven relativistic magnetrons in S-band. This experiment was a successor to a successful two-magnetron experiment done in previous years. Figure 3-2 shows the 4-magnetron configuration. Figure 3-3 is a photo of the 7-magnetron assembly. These seven magnetrons were built into a single module with a common, pulsed power driven vacuum system and magnetic guide field.

The module and the experimental results are described in detail in Appendix B. The net result was that total extracted power was 2 GW with four magnetrons and 2.9 GW with seven magnetrons. One geometry was found to produce qualitatively better phase locking operation than any other: the "hybrid" geometry. This is a maximally-coupled array in which each source is connected to all of its nearest neighbors. The general result is that more connection between the magnetrons produces better phase locking. The phase coherence of the sources was $\pm 20^{\circ}$, which is sufficient to allow coherent superposition of radiation on a target.

Completion of the magnetron module experiment shows that very large powers (~100 GW) could be produced by creating an array of such modules. Therefore, phase locking can be considered to be a demonstrated art in HPM.

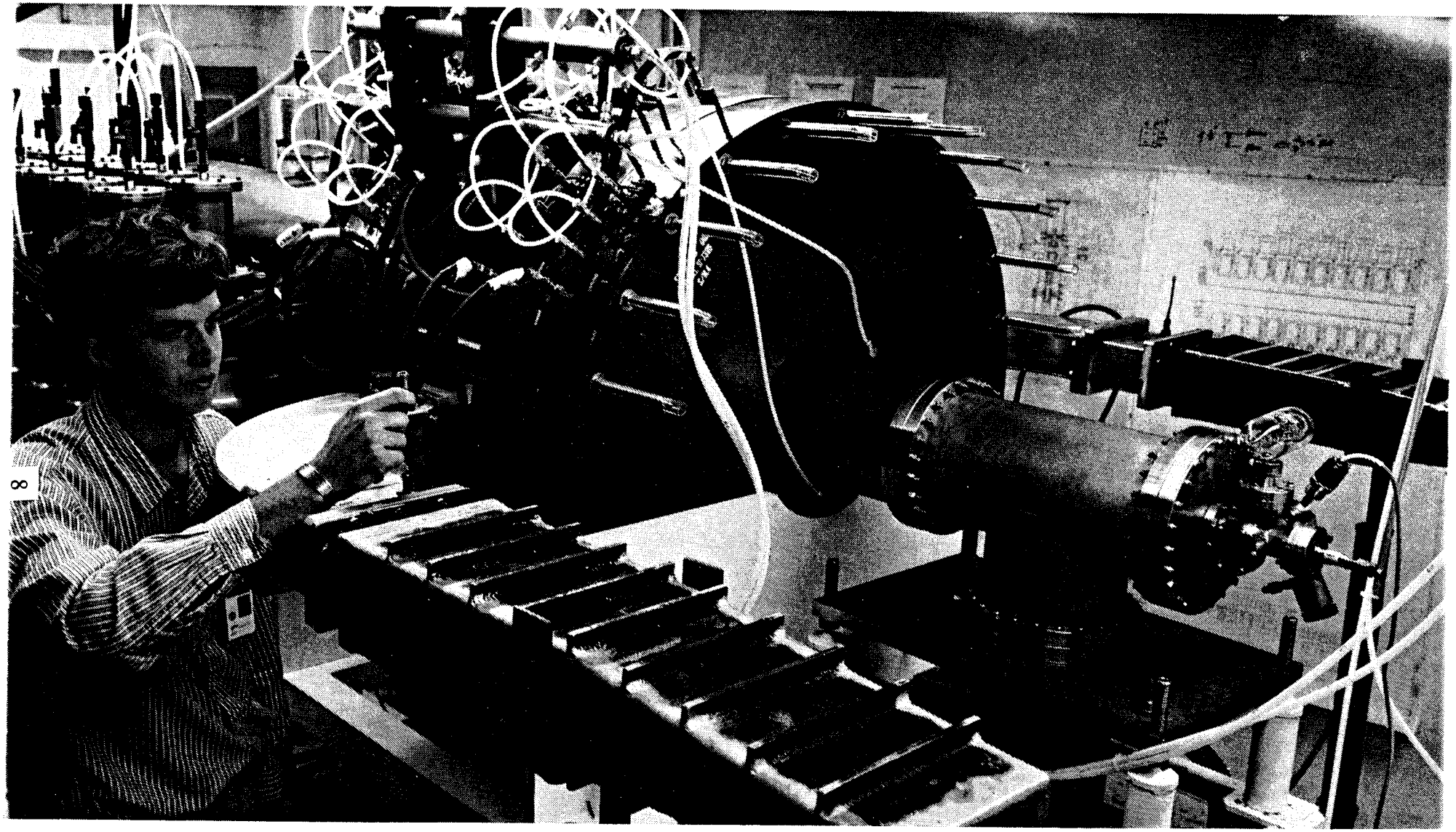

Figure 3-1. **Repetitive L-band magnetron on CLIA (shown in background). The magnetron radiation is extracted in two waveguides and absorbed in loads.**

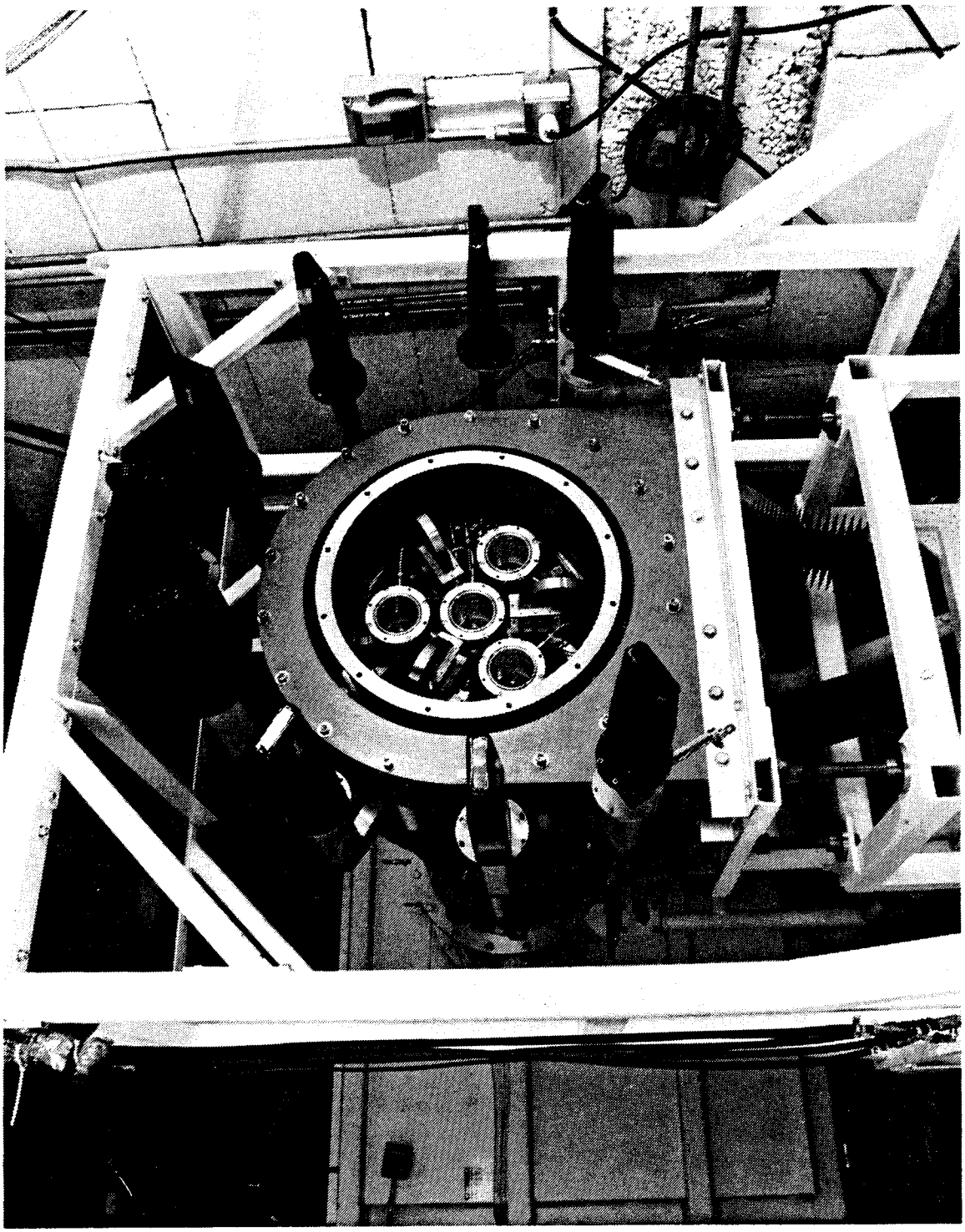

Figure 3-2. Multiple-magnetron phase-locking module with four magnetrons.

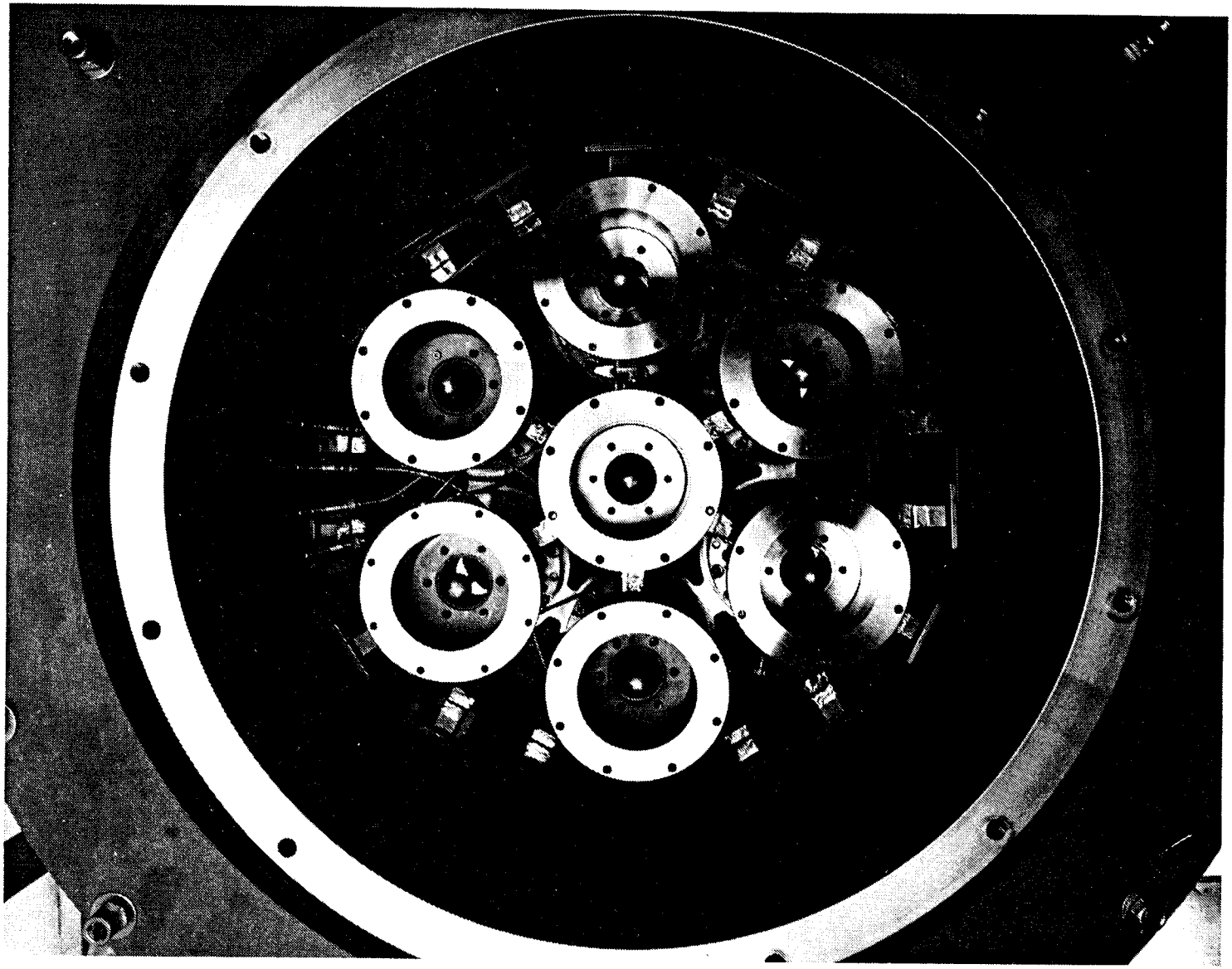

Figure 3-3. Seven-magnetron module in central connection geometry.

SECTION 4

FACILITY UPGRADE AND OPERATION

4.1 HIGH POWER S-BAND FREQUENCY AGILE KLYSTRON.

PI has developed a frequency agile relativistic klystron under its own funding in order to explore this very attractive source type. The Relativistic Klystron Amplifier (RKA) has been used in effects testing described below.

The narrowband HPM sources developed to date are "laboratory prototypes" constructed with limited lifetime components and designed without great attention given to engineering reliability issues. In response to this lack of what could be termed a "deployable" HPM microwave source, Physics International has developed a high power, S-band, klystron that scales conventional klystron (i.e., non-relativistic) technology to the 200 MW level.

The electron gun and seven bunching cavities are patterned after a SLAC design. The general layout is shown in Figure 4-1; Figure 4-2 is a photo of the klystron during assembly. Rather than synchronously tuned, the five bunching cavities are stagger-tuned to produce an instantaneous 10% bandwidth centered at 2.9 GHz. A coupled-cavity output section which feeds a single WR-284 output arm allows microwave extraction across the entire 200 MHz band. The design uses a thermionic cathode, metal-ceramic hydrogen-brazed assemblies and bake-out procedures characteristic of hard vacuum tubes. Sufficient water cooling has been incorporated to permit operation up to 1-μs pulse duration at 100 Hz repetition rates.

Table 4-1 shows the design parameters against the measured parameters during the initial operation. Peak power of 140 MW has been generated at 15% electronic efficiency despite the perveance values being 50% higher than design. Thus far, the device has been operated at 1 Hz repetition rate; however, this does not represent a limit. The klystron amplifies its 1-kW drive signal across its entire instantaneous bandwidth. A spurious competing mode at about 2.9 GHz is also present in all cases. Its cause and subsequent suppression is to be the subject of future research.

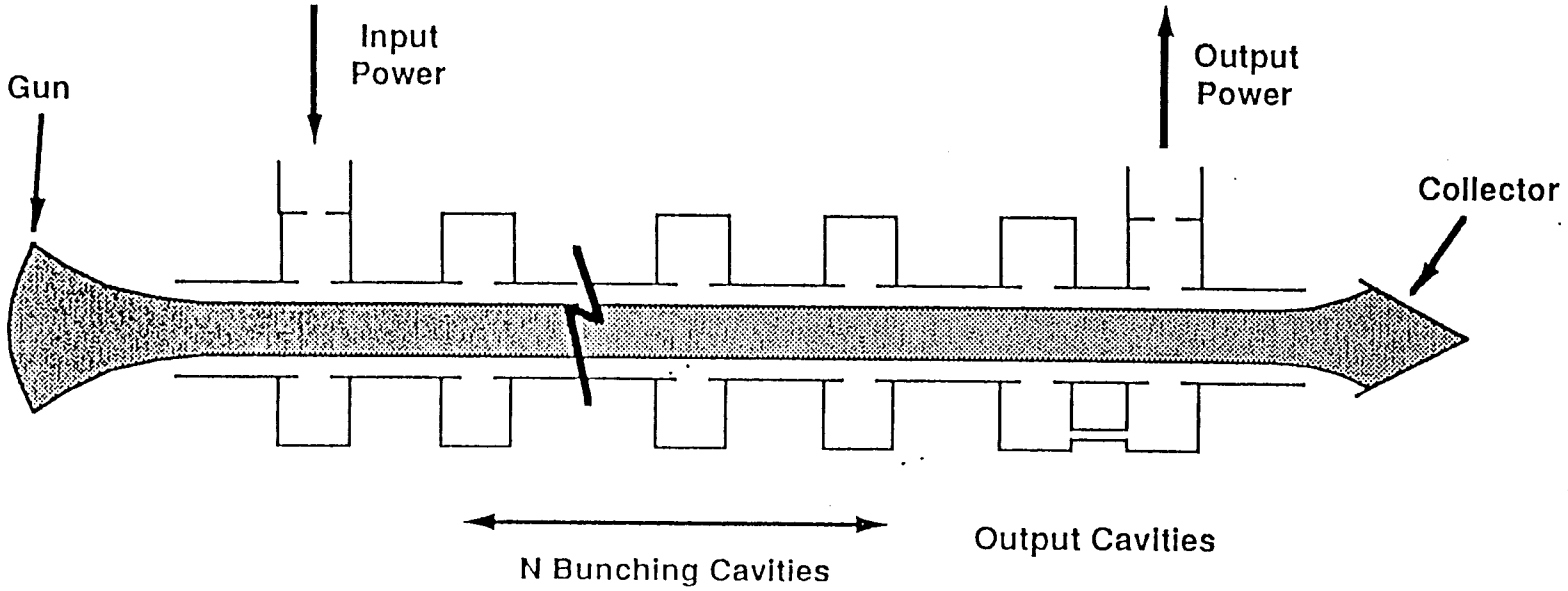

Figure 4-1. Configuration of the S-band broad-bandwidth relativistic klystron.

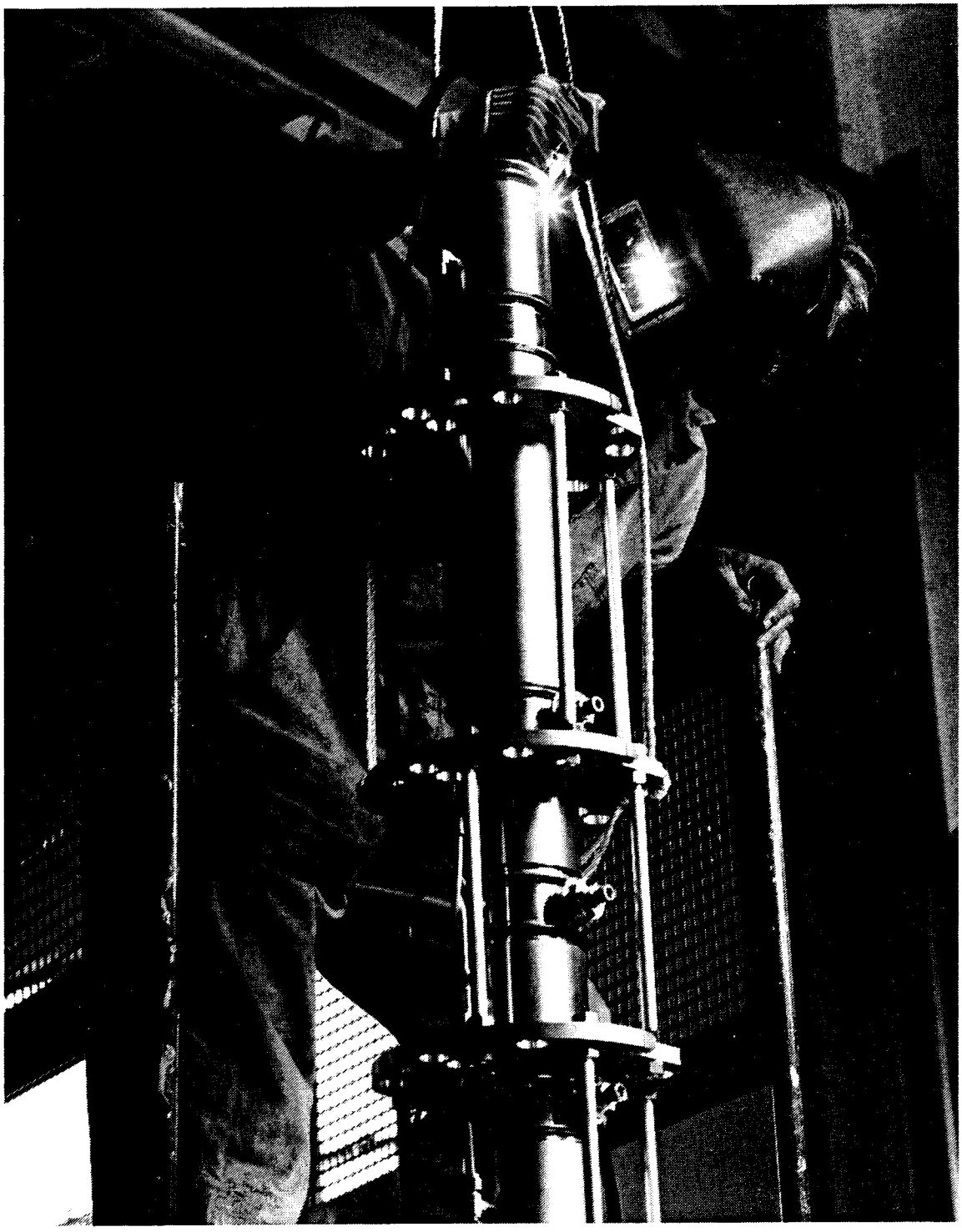

Figure 4-2. S-band relativistic klystron under assembly.

Table 4-1. Design versus measured operational parameters.

Parameter	Design	Measured
Beam Voltage	625 kV	620 ± 20 kV
Collector Current	1.0 kA	1.5 ± .5 kA
Perveance	2.0 μpervs	3.1 ± .9 μpervs
Peak RF Power	250 MW	140 MW (@ 2.9 GHz)
Center Frequency	2.9 GHz	~ 2.85 GHz
Instantaneous Bandwidth	200 MHz	> 200 MHz
Extraction Efficiency	40%	15.1 ± 5.5%

At any given frequency the klystron output is quite stable and reproducible. Figure 4-3 is an overlay of five shots at 2.95 GHz, and 126 MW peak power. The foreshortened pulse (FWHM = 20 ns) is probably due to the lack of a voltage flat top in the 60-ns CLIA drive pulse, which is poorly matched to the klystron impedance.

After the above development of the RKA microwave source, DNA provided funding to connect the source to the anechoic chamber of the DNA/SDI HPM Testing Facility. Microwave waveguide plumbing was installed to connect the output waveguide of the RKA to an evacuated S-band antenna inside the anechoic chamber. The pattern was mapped and showed a standard TE10 radiation pattern.

After operation of the source in the facility, tests were initiated using the RKA. The object irradiated was the Pershing Missile GIEU system. The results of this test have been reported separately by Jaycor.

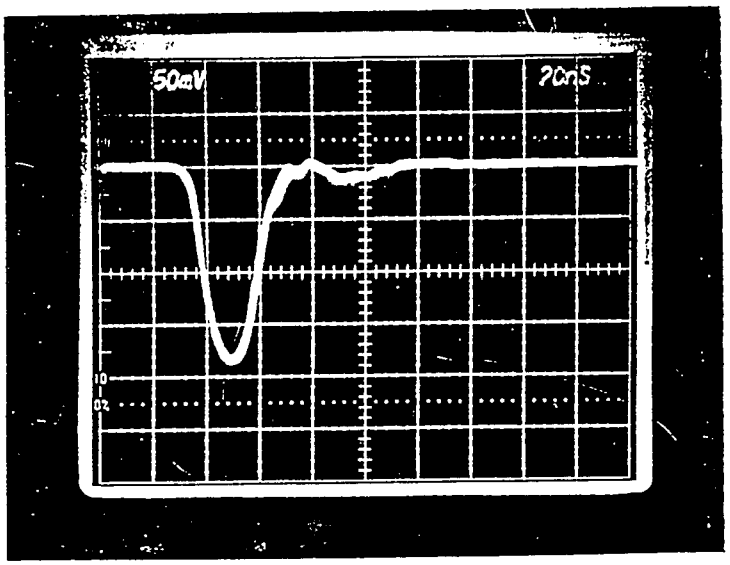

Figure 4-3. Five shot overlay at ~ 1pps. (Frequency = 2.95 GHz, Peak Power = 126 MV, FWHM = 20 ns.)

APPENDIX A

PULSED POWER PAPER

CLIA - A COMPACT LINEAR INDUCTION ACCELERATOR SYSTEM

S. Ashby, D. Drury, G. James, P. Sincerny, L. Thompson

Physics International Company
2700 Merced Street
San Leandro, California 94577

L. Schlitt

Leland Schlitt Consulting Services
Livermore, California

Abstract

CLIA (Compact Linear Induction Accelerator) is a 750-kV, 10-kA, 60-ns, 100-Hz driver in use at Physics International Company. The design and operational characteristics of the accelerator will be described in this paper.

The CLIA system consists of a ten-cell accelerator with a cathode stalk to sum the voltage up to a single diode load, ten magnetically switched water insulated PFLs, a single two-stage magnetic compression unit (MCU) to charge the PFLs, and thyratron switched intermediate energy store (IES) and command resonant charge (CRC) units to drive the MCU.

A linear induction accelerator system permits all pulse compression to be done at moderate voltage (40 to 150 kV) and then uses the accelerator structure to add parallel voltage pulses into a single high voltage output (750 kV). This technique allows the switching to be done at moderate voltage and also makes the use of hydrogen thyratrons and magnetic switches possible.

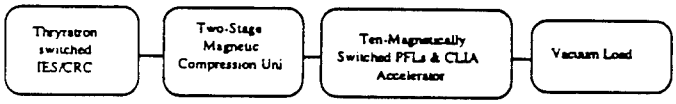

Figure 1. Block diagram of CLIA system.

Figure 1 is a block diagram of the power chain of CLIA. The energy compression chain begins with a 300-kW, 50-kV dc-power supply. This power supply charges a filter bank to 40 kV. Energy is extracted from this bank, switched, and compressed in time by thyratron switched CRC and IES circuits. The output of these units charges the MCU . The two-stage MCU further compresses the energy and raises the voltage using magnetic switching and a 2:1 transformer. The output of the MCU charges ten-parallel water dielectric PFLs. These PFLs then discharge through magnetic switches into the accelerator, where the voltages are summed to produce the 750-kV output. This 750-kV, 10-kA pulse is used to drive the vacuum load.

The full system has been tested to average power levels exceeding its design specifications. Repetition rates of 250 Hz at over 600 kV matched load voltage have been achieved.

The system from the PFLs back toward the power supply has been designed with 65% more energy than believed necessary to charge the PFLs. This increase in energy was done to allow for a subsequent increase in pulse length to 100 ns if the modelling was correct or to overcome losses in excess of what was modelled if the modelling was incorrect.

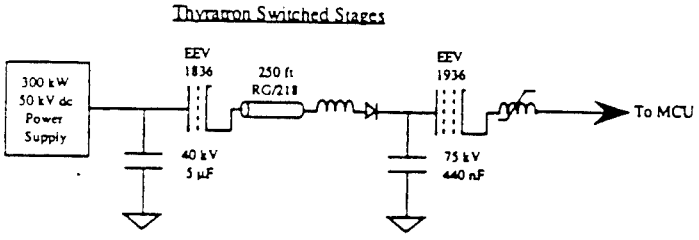

Figure 2. Schematic of IES/CRC circuit.

Figure 2 is a schematic of the power supply/IES/CRC circuit. The first capacitor is the filter bank. It is switched through an EEV 1836 hydrogen thyratron into the IES capacitor. The 250 foot length of cable is necessary because the two sections of this circuit will be physically located 250 feet apart. The CRC circuit rings the IES capacitor up to 75 kV in about 100 μs. This capacitor is then switched by an EEV 1936 tube into the MCU. The magnetic switch shown in the schematic acts as a diode to prevent reverse current through the thyratron. This circuit was originally tested with a resistive load on the output for a 200-Hz, 5-second run at 75-kV output voltage and has been used at 250 Hz into the MCU. This circuit can deliver more than 1.2 kJ per pulse for an average power of over 240 kW. Representative waveforms are shown in Figure 3.

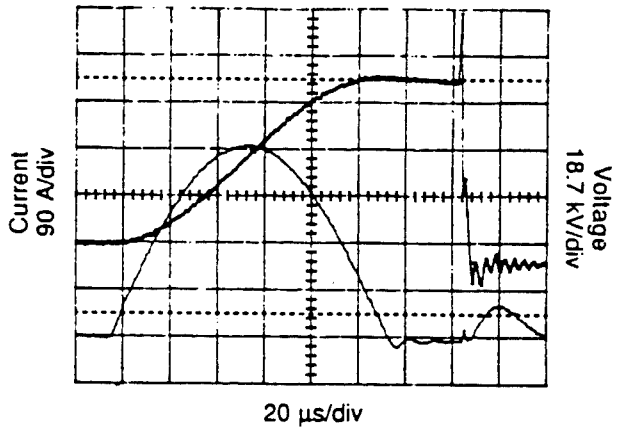

Figure 3. IES capacitor voltage and charging current waveforms at 38 kV filter bank charge.

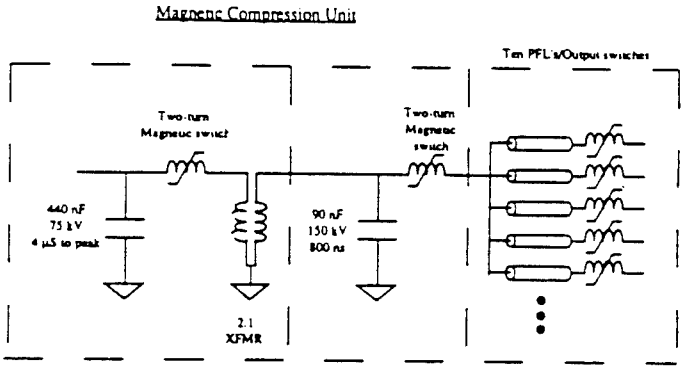

Figure 4. Schematic of the MCU and PFLs.

Figure 4 is a schematic of the next part of the system, the MCU and PFLs. The energy from the IES comes in on the left, charging the first capacitor to 75 kV in about 4 μs. This capacitor is discharged by a two-turn magnetic switch into a 2:1 inverting transformer. The output of this transformer charges a 90 nF water capacitor to 150 kV. This capacitor discharges through another two-turn magnetic switch into the ten parallel PFLs. This entire assembly, except for the PFLs, fits in two tubes each approximately 50 cm in diameter and 1.5 meters long.

The PFLs are of a 6.8 ohm water-insulated coaxial design. The PFLs are charged to 150 kV each to form the 75-kV, 60-ns output pulse. Each has its own magnetic switch on the output. The output of the switch feeds directly into the accelerator.

The magnetic switches and transformer core are made of Allied Metglas 2605CO tape. The thickness of tape used varies from 1 mil in the first-stage switch to 0.6 mil in the PFL output switch. A model has been developed to predict the performance of these cores which includes the effects of changes in shape of the BH loop with different rates of magnetization as are found in a pulse compression chain.

Waveforms achieved in operation of this MCU are shown in Figure 5.

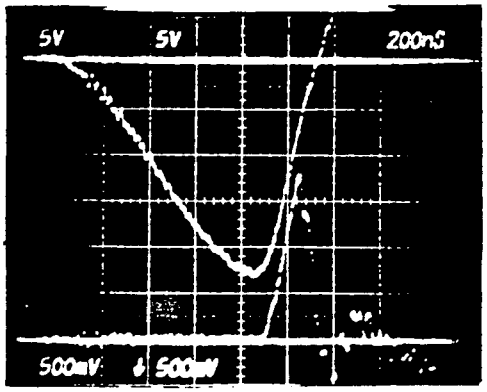

Water Capacitor Voltage, 28.5 kV/div

PFL Voltage, Uncalibrated

200 ns/div

Figure 5. MCU waveforms at 30 kV filter charge.

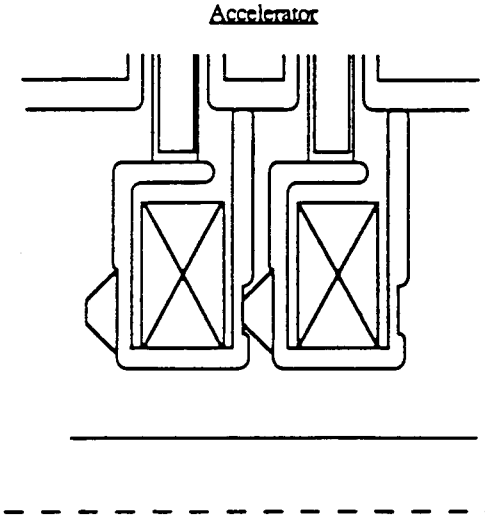

Figure 6. Cross section of the CLIA accelerator structure.

Figure 6 is a section through the accelerator, showing two of the ten cells. The inner diameter of the core is 8.5 inches. The width of the cores is 2 inches. The cores are wound from 0.6 mil 2605CO Metglas with 3.5 micron mylar insulation. The outer radius of the core is 15.5 inches. A cathode stalk runs up the center of the accelerator and the full diode voltage appears across the A-K gap at the load end. The actual effective length of each cell is 10 cm, giving an accelerator gradient of 0.75 MV/meter.

Testing

The CLIA system was first fired into a resistive load, which also functioned as a load voltage monitor. A Rogowski current monitor was placed around this monitor to measure the load current. Repetition rate was limited in this configuration due to the capability of the load to absorb energy, but it allowed us to accurately measure the load voltage, a task that is difficult with a vacuum load in place. Waveforms obtained in this stage of testing are given in Figure 7.

After the system was characterized into a resistive load, an e-beam diode was placed on the output end to allow repetitive operation. Various voltages and repetition rates were tested. There were two limits to the average power achievable. First, the dc power supply used limited the input power available to the CRC. Secondly, we experienced some breakdowns late in time in the water capacitor in the MCU. These breakdowns limited the output voltage to 650 kV

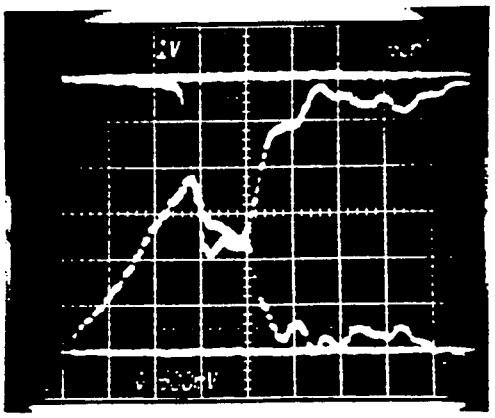

PFL voltage 28 kV/div
Output voltage 167 kV/div
50 ns/div

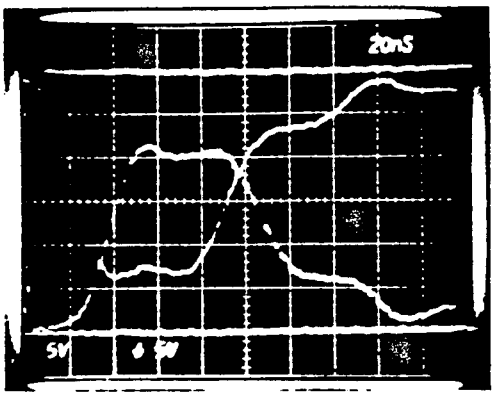

Output current shunts 1 kA/div
20 ns/div

Figure 7. Waveforms during resistive load testing.

into a matched load. A burst of 100 shots at 250 Hz has been fired at this level, yielding 85 kW average electrical output power. Longer bursts should be possible but have not yet been demonstrated. Figure 8 shows the current waveform at the output from CLIA during a 50-shot, 100-Hz run. The uniformity shot-to-shot is very good.

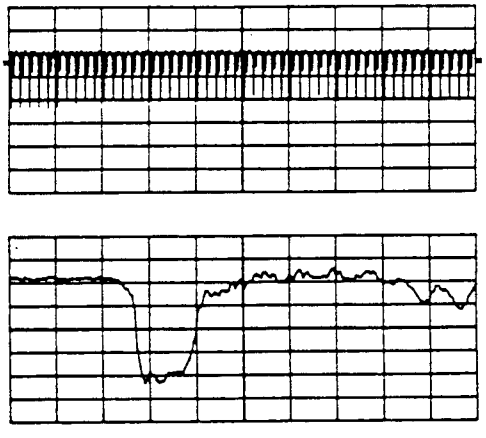

50 Current Pulses
5 kA/div

Pulse No. 27
2 kA/div

50 ns/div

Figure 8. Output current of CLIA for 100 Hz, 50 shot run.

Reset

The magnetic cores of the system are reset by means of dc current applied through high-voltage inductors. This current is applied at two different locations. A connection immediately after the second thyratron switch provides current to reset the magnetic assist switch, the first-stage MCU switch, and the primary of the transformer. A second current is applied at the point between the water capacitor and the second-stage switch to reset the secondary of the transformer, the second-stage switch, the PFL output switches, and the accelerator cores. This second current must provide current to eleven different paths to ground and current sharing between these paths has been ensured by using thinwall stainless-steel tubing to make some of the components in these paths to provide resistance.

During testing, various reset current levels were used at various voltage and repetition rates. If insufficient current was used to reset the accelerator cores, an interesting effect was observed. The output pulse would gently degrade pulse-by-pulse over the span of about 50 pulses until it disappeared; that is, the effect of insufficient reset was not immediate on the next pulse but was a cumulative effect over many pulses. Our higher power runs used reset currents of 500 A dc at the second location and about 50 A dc at the first.

Summary

In CLIA, we have developed a reliable, moderate repetition rate, high average power generator that should be useful to perform repetitive vacuum load research in the future.

APPENDIX B

SOURCE DEVELOPMENT PAPERS

High Peak and Average Power with an L-Band Relativistic Magnetron on CLIA

Steve Ashby, Richard R. Smith, Norman Aiello, James N. Benford, *Senior Member, IEEE*, Nicholas Cooksey, David V. Drury, Bruce D. Harteneck, Jerrold S. Levine, Peter Sincerny, Lance Thompson, and Leland Schlitt

Abstract—**CLIA (Compact Linear Induction Accelerator) is a 750 kV, 10 kA pulse-power generator using magnetic switching to produce 60-ns-long pulses at 200 Hz (90 kW average power) for longer than 1 s. As a first application, we used CLIA to drive an *L*-band magnetron. We observed that the magnetron was capable of consistent operation at repetition rates as high as 250 Hz with no breakdown or pulse-shortening induced by gas buildup or electrode erosion. As the repetition rate exceeded 100 Hz, the average power increased even as the peak power decreased, producing 1 GW peak power and 4.4 kW average power at 100 Hz and 600 MW peak and 6.3 kW average at 250 Hz. A short burst at a 1 kHz repetition rate indicated the possibility of 25 kW average microwave power operation.**

I. Introduction

THE generation of microwaves at high power (>100 MW) has progressed largely on single-shot devices. Yet many applications will require repetitive operation at substantial repetition rates [1], implying high average power. Fig. 1 shows that only a few repetitive high-power experiments have been conducted. In most, the pulse duration was <50 ns, so average powers have been less than 1 kW. Conventional microwave tubes have operated at high average power, but peak power has been low. A notable exception is the klystron developed by Lee *et al.* [2], which was extrapolated from SLAC (Stanford Linear Accelerator Center) klystron technology. This device operated at 150 MW peak power, 1 μs duration, and 150 Hz, to give an average power of 22 kW. Fig. 2 shows the domains of the two technologies. The results of the experiments described here are displayed in Figs. 1 and 2.

The technical challenge of achieving both high peak and high average power is that repetitive operation may: (i) evolve material from surfaces which raise the pressure, causing breakdown in the high electric fields (~100 kV/cm) of successive pulses; and (ii) prevent emission of electron beams from cold cathode surfaces by evaporating monolayers (of gas, oil, water, etc.) and firing again before they can recondense. (It has been suggested that monolayers are the seat of plasma formation from cold cathodes, rather than plasma formation from exploded metal micro-projections.) The vacuum poisoning issue can be addressed by better high-vacuum techniques, but only by actually operating at high peak power (>100 MW) and high repetition rates (>100 Hz) can the practical limitations be found.

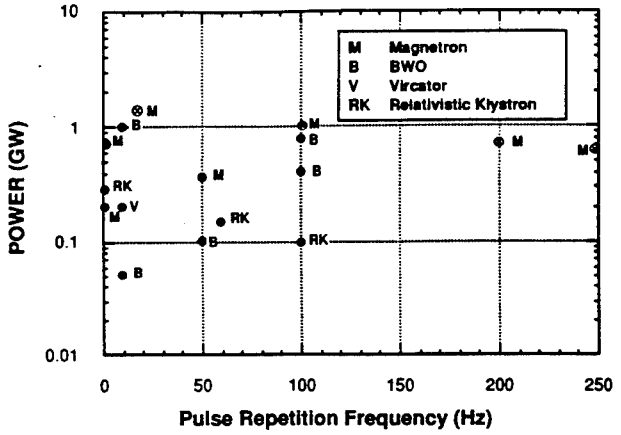

Fig. 1. Summary of high-power repetitive microwave source capability. The highlighted points are results from the present experiment.

A particularly attractive pulsed-power system for such experiments is the hard-core (i.e., central cathode shank, not e-beams) linear-induction accelerator (LIA), first used in high-power microwave research [3] by the Tomsk group. They operated an *S*-band relativistic magnetron at 300 MW, 60 ns, 50 Hz, for an average power of 0.5 kW. The system is compact, which is an advantage for most applications. The basic reason for the compactness is that voltage from individual sections is added in vacuum so that the peak voltage appears only on the load. The system we describe here, CLIA (Compact Linear Induction Accelerator), is an LIA using magnetic pulse compression for switching. This technology has an inherent long lifetime, eliminating the erosion problems of spark gaps. The first microwave source tested on CLIA was an *L*-band relativistic magnetron. Our goal was to produce a pulse train of 100 shots at 100 Hz, each with peak power of 1 GW. This far extends the experience of 1–10 Hz sustained operation [4], [5], 50-Hz continuous operation [3], and the three shot bursts at 100–160 Hz [6] previously reported, producing high peak and average microwave power simultaneously. We are now operating relativistic klystrons on CLIA. In this paper we

Manuscript received September 27, 1991; revised January 27, 1992. This work was supported by the Defense Nuclear Agency and the Strategic Defense Initiative Office under a contract managed by H. Brandt of the Harry Diamond Laboratory.

S. Ashby, R. R. Smith, N. Aiello, J. N. Benford, N. Cooksey, D. V. Drury, B. D. Harteneck, J. S. Levine, P. Sincerny, and L. Thompson are with the Physics International Company, San Leandro, CA 94577.

L. Schlitt is with Leland Schlitt Consulting Services, Livermore, CA.

IEEE Log Number 9108108.

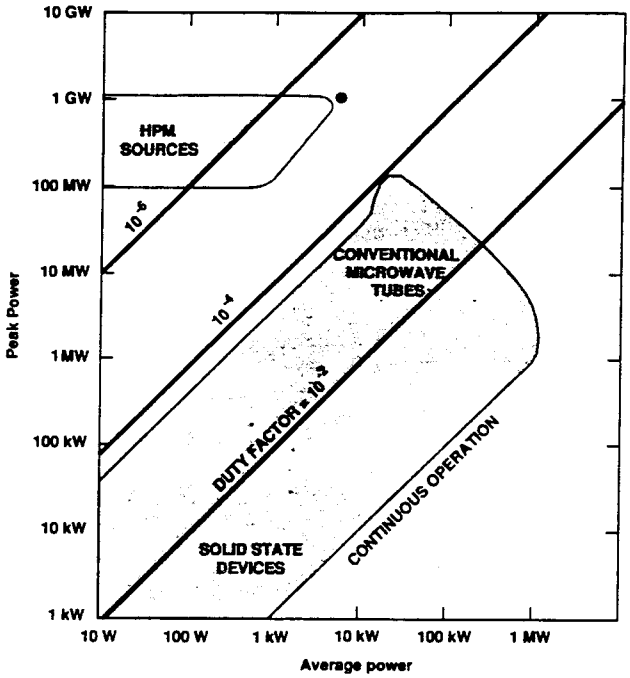

Fig. 2. Peak versus average power domains for conventional and HPM sources. The highlighted point is from the experiment reported here.

describe the CLIA pulse-power system and report the results of the L-band magnetron experiment.

II. CLIA System

A. Description

The CLIA system consists of a ten-cell accelerator (shown in Fig. 3) with a cathode stalk to sum the voltage up to a single diode load, ten magnetically switched water-insulated PFL's, a single two-stage magnetic compression unit (MCU) to charge the PFL's, and thyratron-switched intermediate energy store (IES) and command resonant charge (CRC) units to drive the MCU.

A linear-induction accelerator system permits all pulse compression to be done at moderate voltage (40 to 150 kV), and then uses the accelerator structure to add parallel voltage pulses into a single high-voltage output (750 kV). This technique allows the switching to be done at moderate voltage and also makes the use of hydrogen thyratrons and magnetic switches possible.

Fig. 4 is a block diagram of the power chain of CLIA. The energy-compression chain begins with a 300 kW, 50 kV dc-power supply. This power supply charges a filter bank to 40 kV. Energy is extracted from this bank, switched, and compressed in time by thyratron-switched CRC and IES circuits. The output of these units charges the MCU. The two-stage MCU further compresses the energy and raises the voltage using magnetic switching and a 2 : 1 transformer. The output of the MCU charges ten-parallel water dielectric PFL's. These PFL's then discharge through magnetic switches into the accelerator, where the voltages are summed to produce the 750 kV output. This 750 kV, 10 kA pulse is used to drive the vacuum load.

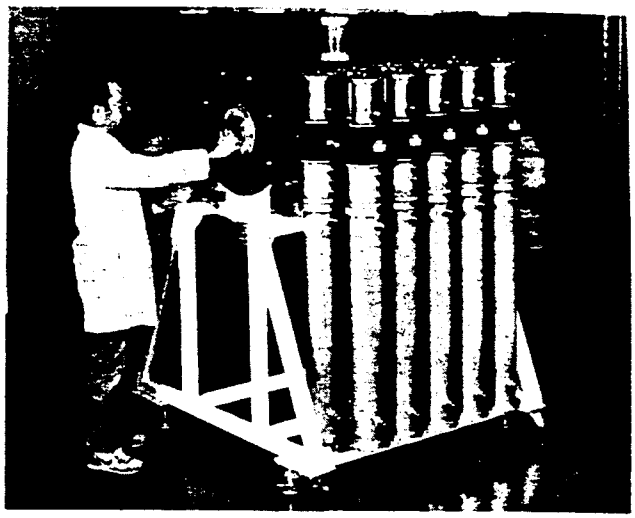

Fig. 3. Photograph of the CLIA PFL's and accelerator sections.

The full system has been tested to average power levels exceeding its design specifications. Repetition rates of 250 kHz at over 600 kV matched-load voltage have been achieved.

The system from the PFL's back toward the power supply has been designed with 65% more energy than believed necessary to charge the PFL's. This increase in energy was done to allow for a subsequent increase in pulse length to 100 ns if the modeling was correct, or to overcome losses in excess of what was modeled if the modeling was incorrect.

Fig. 5 is a schematic of the power supply/IES/CRC circuit. The first capacitor is the filter bank. It is switched through an EEV 1836 hydrogen thyratron into the IES capacitor. The 250 ft length of cable is necessary because the two sections of this circuit are physically located 250 ft apart. The CRC circuit rings the IES capacitor up to 75 kV in about 100 μs. This capacitor is then switched by an EEV 1936 tube into the MCU. The magnetic switch shown in the schematic acts as a diode to prevent reverse current through the thyratron. This circuit was originally tested with a resistive load on the output for a 200 Hz, 5 s run at 75 kV output voltage, and has been used at 250 Hz into the MCU. This circuit can deliver more than 1.2 kJ per pulse for an average power of over 240 kW. Representative waveforms are shown in Fig. 6.

Fig. 7 is a schematic of the next part of the system, the MCU and PFL's. The energy from the IES comes in on the left, charging the first capacitor to 75 kV in about 4 μs. This capacitor is discharged by a two-turn magnetic switch into a 2 : 1 inverting transformer. The output of this transformer charges a 90 nF water capacitor to 150 kV. This capacitor discharges through another two-turn magnetic switch into the ten parallel PFL's. This entire assembly, except for the PFL's, fits in two tubes each approximately 50 cm in diameter and 1.5 m long.

The PFL's are of a 6.8 Ω water-insulated coaxial design. The PFL's are charged to 150 kV each to form the 75 kV, 60 ns output pulse. Each has its own magnetic switch on the output. The output of the switch feeds directly into the accelerator.

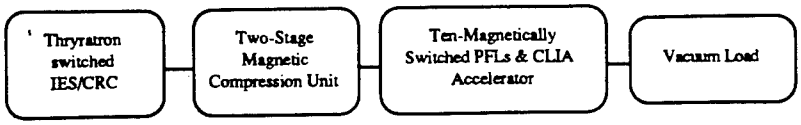

Fig. 4. Block diagram of the CLIA system.

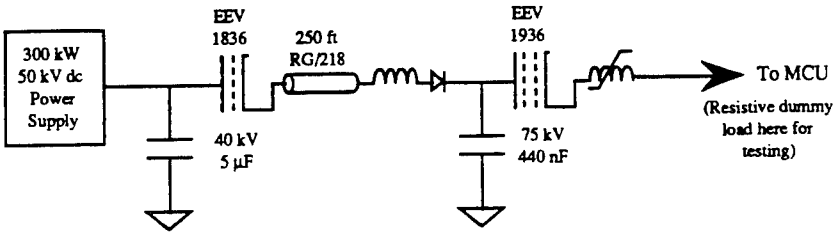

Fig. 5. Schematic of the IES/CRC circuit.

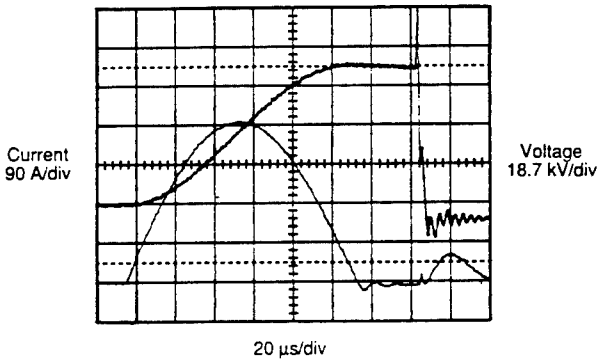

Fig. 6. IES capacitor voltage (upper trace, right-hand scale) and charging current (lower trace, left-hand scale) waveforms at 38 kV filter bank charge.

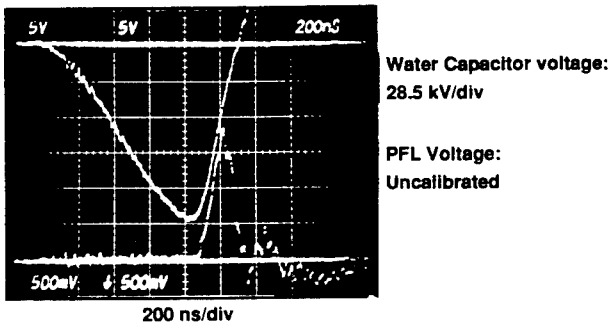

Fig. 8. MCU waveforms at 30 kV filter charge.

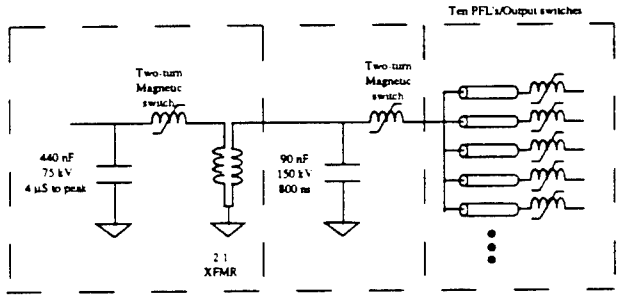

Fig. 7. Schematic of the MCU and PFL's.

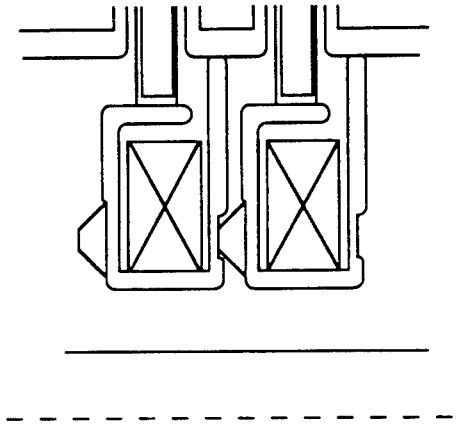

Fig. 9. Cross section of the CLIA accelerator structure.

The magnetic switches and transformer core are made of Allied Metglas 2605CO tape. The thickness of tape used varies from 1 mil in the first-stage switch to 0.6 mil in the PFL output switch. A model has been developed to predict the performance of these cores, which includes the effects of changes in shape of the BH loop with different rates of magnetization as are found in a pulse-compression chain. Waveforms achieved in operation of this MCU are shown in Fig. 8.

Fig. 9 is a section through the accelerator, showing two of the ten cells. The inner diameter of the core is 8.5 in. The width of the cores is 2 in. The cores are wound from 0.6 mil 2605CO Metglas with 3.5 μm Mylar insulation. The outer radius of the core is 15.5 in. A cathode stalk runs up the center of the accelerator and the full diode voltage appears across the A-K gap at the load end. The actual effective length of each cell is 10 cm, giving an accelerator gradient of 0.75 MV/m.

The magnetic cores of the system are reset by means of dc current applied through high-voltage inductors. This current is applied at two different locations. A connection immediately after the second thyratron switch provides current to reset the magnetic assist switch, the first-stage MCU switch, and the primary of the transformer. A second current is applied at the point between the water capacitor and the second-stage

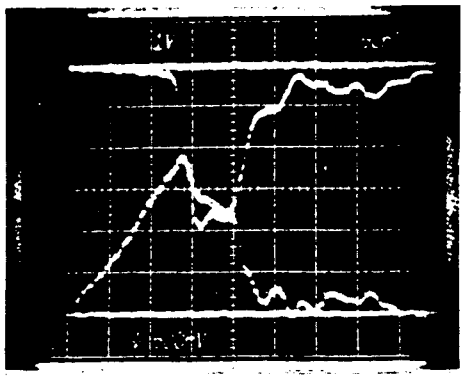

PFL voltage: 28 kV/div
Output voltage: 167 kV/div50 ns/div

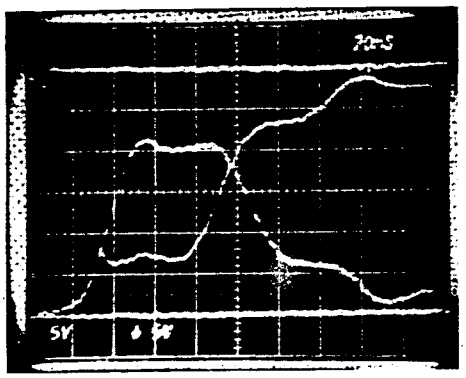

Output current shunts: 1 kA/div 20ns/div

Fig. 10. Waveforms during resistive load testing.

switch to reset the secondary of the transformer, the second-stage switch, the PFL output switches, and the accelerator cores. This second current has 11 different paths to ground; current sharing between these paths has been ensured by using thinwall stainless-steel tubing to make some of the components in these paths, thereby providing resistance.

B. System Tests

The CLIA system was first fired into a resistive load, which also functioned as a load-voltage monitor. A Rogowski current monitor was placed around this monitor to measure the load current. Repetition rate was limited in this configuration due to the capability of the load to absorb energy, but it allowed us to accurately measure the load voltage, a task that is difficult with a vacuum load in place. Waveforms obtained in this stage of testing are given in Fig. 10.

After the system was characterized into a resistive load, an e-beam diode was placed on the output end to allow repetitive operation. Various voltages and repetition rates were tested. There were two limits to the average power achievable. First, the dc-power supply used limited the input power available to the CRC. Secondly, we experienced some breakdowns late in time in the water capacitor in the MCU. These breakdowns limited the output voltage to 650 kV into a matched load. A burst of 100 shots at 250 Hz has been fired at this level, yielding 85 kW average electrical output power. Longer bursts should be possible, but have not yet been demonstrated. Fig. 10 shows the current waveform at the output from CLIA during a 50 shot, 100 Hz run. The shot-to-shot uniformity is very good.

During testing, various reset current levels were used at various voltage and repetition rates. If insufficient current was used to reset the accelerator cores, an interesting effect was observed. The output pulse would gently degrade pulse-by-pulse over the span of about 50 pulses until it disappeared; that is, the effect of insufficient reset was not immediate on the next pulse, but was a cumulative effect over many pulses. Our higher power runs used reset currents of 500 A dc at the second location, and about 50 A dc at the first.

III. Repetitive Magnetron

A. Description

We modified an existing L-band magnetron [7] for repetitive operation for this experiment. It has six cavities, with cathode, anode, and vane radii of 1.27, 3.18, and 8.26 cm, respectively, and oscillated in the π-mode at 1.1 GHz. This magnetron had produced 3.6 GW when connected to Marx bank/water-line drivers. Our expectations were for significantly less power, because the magnetron, at $\sim$25 Ω, is a poor electrical match to CLIA, at 75 Ω.

The modifications for repetitive operation consisted of cooling the anode vanes (via water channels 3 mm below the surface) and the downstream surface where the axial current emitted from the cathode tip is collected. Additionally, we paid particular attention to creating good electrical contact between parts and avoiding virtual leaks. We also used a cryo-pump for our vacuum system to eliminate possible contamination from backstreaming oil. Base pressure was 4×10^{-6} torr. Previous single-shot experiments have shown that peak power is increased by lowering base pressure [8].

As shown in Fig. 11, the microwaves were extracted from two opposing resonators which were connected to the WR650 waveguide through quarter-wave transformers and absorbed by dummy loads, all in vacuum. Power samplers ($\approx$80 dB coupling) allowed for power, pulse shape, and frequency diagnostics. The signal was viewed two ways: by the response of a crystal detector recorded on each pulse, and directly on a high-speed oscilloscope on one pulse (not necessarily the first) within the burst. The only electrical diagnostic used was a Rogowski coil measuring the total current into the magnetron. The voltage was determined from the current, the CLIA charge voltage, and a measured load line.

B. Experimental Results

At a repetition rate of 100 Hz, we produced pulse trains of 1.0 GW, 50 ns FWHM pulses with 44 J each yielding 4.4 kW average power. Fig. 12(a) shows the current and microwave pulse trains (each spike is a separate pulse, the data acquisition system does not record during the time between pulses) for a 50 shot burst; Fig. 12(b) is an expanded view of one pulse in the middle of the burst. The recorded microwave signal is the crystal output on one of two extraction arms. This produces the nonlinear scale for power. To determine the total extracted

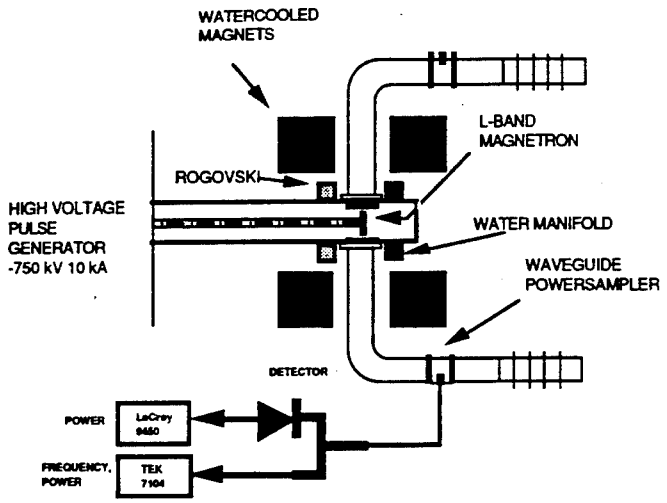

Fig. 11. L-band magnetron CLIA.

power we have doubled the power measured on one arm, since we know, from other measurements, that the two extraction arms have nearly identical powers.

As can be seen from Fig. 12, all the pulses are nearly identical. The microwave pulses last as long as the current pulse; i.e., there is no indication of impedance collapse or shifting of the operating point off resonance (effects conjectured to limit the pulse length in other relativistic magnetron experiments). A significant feature of magnetron operation on CLIA is that the pulse duration of the microwaves (50 ns) is only slightly less than that of the electrical pulse (60 ns). In many previous relativistic magnetron experiments, the ratio is typically 1/3 [9]

The first few pulses are slightly more powerful, because there is slightly more current. This is due to the time it takes to establish a steady state within the CLIA power-conditioning system. This effect becomes more obvious as the repetition rate is increased, causing a decrease in the peak power, even though the average power is still increasing. As shown in Fig. 13, at 200 Hz the typical peak power dropped to 700 kW, while the average power rose to 6.0 kW. At 250 Hz, the trend continued to yield 600 MW peak power and 6.3 kW average power. We tested the system with a 5 shot burst at 1000 Hz (far beyond the average current specification for CLIA) to see if there was a minimum recovery time between pulses. As Fig. 14 illustrates, the magnetron operates at 1000 Hz, even though CLIA is capable of only a few pulses. Therefore the evolved gas clearing time is <1 ms. Based on the third pulse, we estimate that the average power would be $\approx$25 kW, with a peak power of 600 MW. These results are summarized in Table I.

IV. Discussion

The results reported above extend the envelope of high average and high peak powers for microwave sources, as shown in Fig. 2. What may be most notable about these results are the things that didn't limit operation:

- There is no problem of gas buildup in the magnetron that could produce impedance collapse or in other ways interfere with the magnetron resonance.

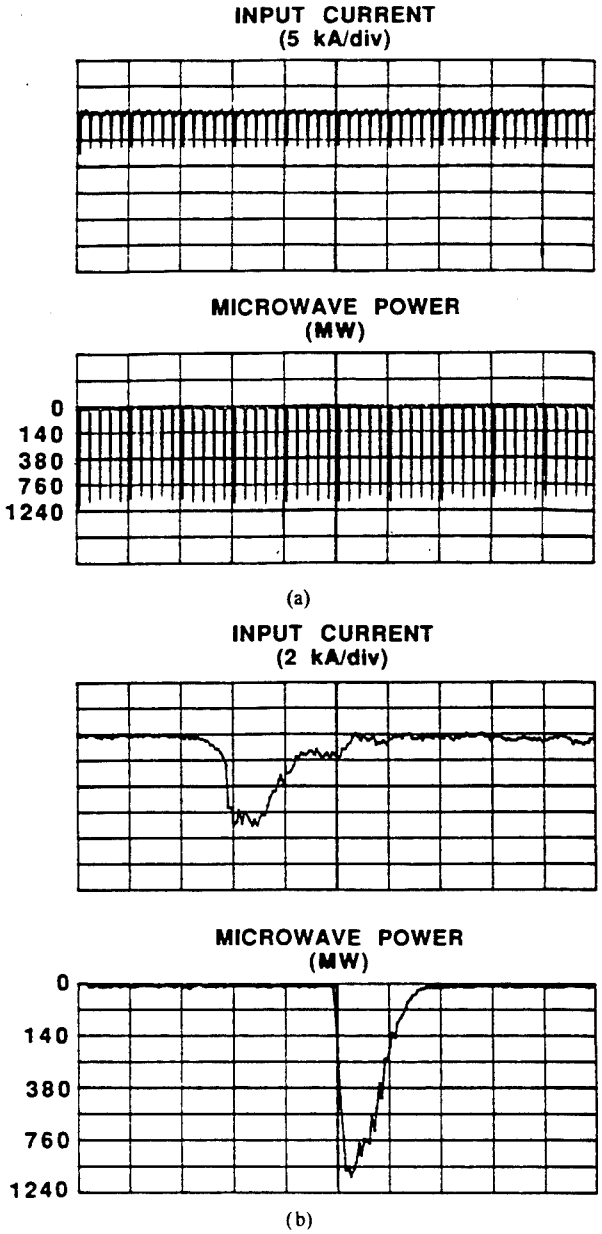

Fig. 12. Current and microwave power for: (a) a 50-shot burst at 100 Hz, and (b) an expanded view of one pulse within the burst.

- At this writing, there is no noticeable erosion of the anode vanes, even after several hundred shots on single-pulse generators and several thousand shots on CLIA, where the anode is water cooled. This is very different from our S- and X-band magnetrons.
- There is no diminution of cold cathode emission after 1000 shots.

CLIA can be upgraded to extend the pulse length beyond the present capability. Since the microwave pulse lasts as long as the current pulse, there is clearly no impedance collapse, and furthermore, there must be relative insensitivity to the applied voltage. Thus there is cause for optimism that this magnetron would generate longer microwave pulses.

In the magnetron, beam emission, RF generation, and beam collection all occur in the same space. This is very different from the linear beam devices such as the relativistic

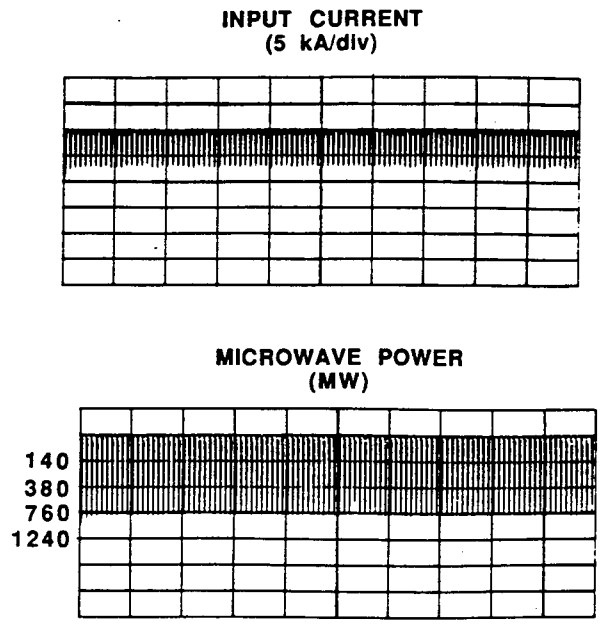

Fig. 13. Current and microwave power for a 100-shot burst at 200 Hz.

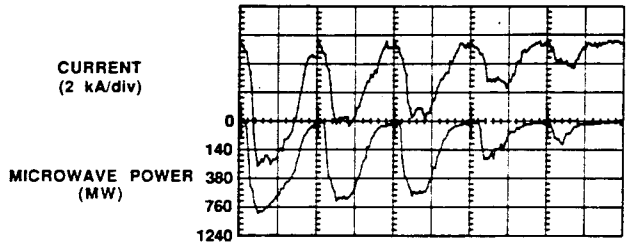

Fig. 14. Current and microwave power for a 5-shot burst at 1000 Hz.

TABLE I
SUMMARY OF MAGNETRON PEAK AND AVERAGE POWER AS A FUNCTION OF REPETITION RATE

Repetition Rate (Hz)	Peak Power (MW)	Average Power (kW)	Number of Shots
100	1000	4.4	50
200	700	6.0	100
250	600	6.3	100
1000*	600	25	5

*Based on third shot of 5 shot sequence.

klystron, traveling wave tube, backward-wave oscillator, and free-electron maser. The problems of repetitive operation are much more difficult in the magnetron because of the proximity of the three functions. Therefore the result of this experiment, that 250 Hz, 100 shot bursts and 1000 Hz, 5 shot bursts can be achieved reproducibly, indicates that much higher average powers should be achievable in the magnetron and other high peak-power devices at repetition rates in excess of a kilohertz.

REFERENCES

[1] J. Benford and J. Swegle, *High Power Microwaves*. Boston: Artech, 1992.

[2] T. Lee, G. Konrad, Y. Okazaki, M. Watanabe, and H. Yonezawa, "Design and performance of a 150-MW klystron at *S*-band", *IEEE Trans. Plasma Sci.*, vol. PS-13, p. 545, 1985.

[3] V. V. Vasil 'yev *et al.*, "Relativistic magnetron operating in the mode of a train of pulses", *Sov. Tech. Phys. Lett.*, vol. 13, p. 762, 1987.

[4] D. Phelps, M. Estrin, J. Woodruff, R. Sprout, and C. Wharton, "Observations of a repeatable rep-rate IREB HPM tube", in *Proc. 7th Int. Conf. on High-Power Particle Beams* (Karlsruhe), 1988, p. 1347.

[5] S. T. Spang *et al.*, "Relativistic magnetron development for use in a lightweight, repetitively pulsed, portable HPM transmitter", *IEEE Trans. Plasma Sci.*, vol. 18, p. 586, 1990.

[6] A. N. Didenko *et al.*, "Pulse-periodic relativistic magnetron", in *Proc. 7th Int. Conf. on High-Power Particle Beams* (Karlsruhe), 1988, p. 1380.

[7] R. R. Smith, J. Benford, B. Harteneck, and H. Sze, "Development and test of an *L*-band magnetron", *IEEE Trans. Plasma Sci.*, vol. 19, p. 628, 1991.

[8] R. Smith *et al.*, "Operation of an *L*-band relativistic magnetron at 100 Hz", in *Intense Microwave and Particle Beams*, vol. II, H. Brandt, Ed., *SPIE*, vol. 1407, p. 83, 1991.

[9] J. Benford and J. Swegle, "Crossed-field devices", in *High Power Microwaves*. Boston: Artech, 1992, chap. 6.

Steve Ashby received the B.S. degree in physics from the University of Illinois.

He is a staff Engineer at Physics International Company, San Leandro, CA. He has over 12 years experience designing and testing large pulsed-power generators. He was Testing Manager of the EAGLE facility and made major contributions to achieving simultaneous switching on Double-EAGLE. More recently, he was Technical Manager on the CLIA pulsed-power program, and is currently the key electrical engineer on the DECADE program. His expertise includes pulsed-power switching, repetitive switching, and dielectric breakdown.

Richard R. Smith, photograph and biography not available at the time of publication.

Norman Aiello received the B.S. degree in mechanical engineering technology from Cogswell College, San Francisco, CA.

He is a Quality Engineer with Physics International Company, San Leandro, CA. Coming from his background and experience in high-power microwave, his current focus is on quality assurance for an electromagnetic launcher pulsed-power system. His specialty is deliverable hardware.

James N. Benford (SM'91) received the M.S. and Ph.D. degrees in physics from the University of California, San Diego, and the B.S. degree in physics from the University of Oklahoma.

He is the Director of the High Power Microwave Division at Physics International Company, Olin Corporation, San Leandro, CA. He has been conducting research in the field of high-power microwaves for the last ten years. Over the last 22 years at Physics International, he has also been the Technical Director and Program Manager of many major experimental programs in high-power microwaves, electron-beam fusion research, and beam-propagation physics. He has also been involved in system analysis and design programs on linear-induction accelerators, pulsed-power generators, beam and plasma experiments, fusion reactor studies, and other pulsed power research. He has over 25 publications in scientific journals and proceedings in the field of high-power microwaves. He is co-author of *High Power Microwaves* (Artech House, 1992).

Nicholas Cooksey, photograph and biography not available at the time of publication.

David V. Drury received the B.S. and M.E.T. degrees from Cogswell Polytechnical College, San Francisco, CA.

He is a Mechanical Engineer with Physics International Company, San Leandro, CA. He has over 14 years experience in the design, construction, fielding, and testing of complex mechanical hardware systems. He was responsible most recently for the design and fabrication of FALCON, DPM, and DPM2. Prior to these tasks, he participated in the conceptual design of the RETF machine.

Bruce D. Harteneck received the B.A. degree in physics from California State University, San Jose, in 1976.

He joined Physics International Company, San Leandro, CA, in 1977, and has worked on a wide variety of projects in the last 14 years, including inertial confinement fusion, X-ray lithography, and pulsed laser holography. Over the last six years he has concentrated on the development of high-power microwave sources. He has over ten publications in scientific journals and proceedings relating to high-power microwave source development.

Jerrold S. Levine received the Ph.D. degree in applied physics from Stanford University in 1981.

After working in the fields of gyrotron development and electron-cyclotron heating of tokamak plasma, he joined Physics International Company, in 1984. He has worked there on projects in radiation simulation using bremsstrahlung and Z-pinch sources, pulsed-power design, inductive energy store/fast opening switches, and X-ray lasers. His recent concentration on high-power microwave sources involves phase-locked arrays of relativistic magnetrons and repetitively pulsed, high-current relativistic klystron amplifiers.

Peter Sincerny received the M.S. and Ph.D. degrees in physics from Lehigh University.

He is the Director of the Advanced Simulator Division, Physics International Company, San Leandro, CA. He has over 11 years of experience in pulsed power and plasma physics. In the past three years as A.S.D. Director, he has managed numerous research and development contracts, with DECADE his primary focus for the past two years. He is responsible for the Advanced Pulsed Power Program technical objective—the opening switch test load—and has also spearheaded bremsstrahlung X-ray source research and development. He is in addition the Director of Operations and Maintenance for the PI-DNA Double EAGLE facility.

Lance Thompson, photograph and biography not available at the time of publication.

Leland Schlitt, photograph and biography not available at the time of publication.

Techniques for High Power Microwave Sources at High Average Power

James N. Benford, *Senior Member, IEEE,* Nicholas J. Cooksey, Jerrold S. Levine, and Richard R. Smith

Abstract— **Generation of microwaves at high power has progressed largely on single shot devices. Applications, however, require high average power, implying operation at substantial repetition rates. This is in a new domain for microwave devices. The technical challenge is to achieve very high electric fields in the source on a repetitive basis without breakdown. We describe experiments on CLIA, a Compact Linear Induction Accelerator, capable of generating 750 kV and 10 kA into a matched load using magnetic switching to produce 60 ns long pulses. As a first application we used CLIA to drive a water-cooled *L*-band magnetron at repetition rates as high as 250 Hz with no breakdown or pulse shortening. This gave 6.3 kW average power. A short burst at 1 kHz demonstrated operation that would translate to an average power of ≈25 kW. In this regime operation is not limited by gas build-up, electrode erosion or microwhisker depletion. We are now operating on CLIA with a high current relativistic klystron. Beams with modulated current powers of ≈1 GW have been generated at 100 Hz for bursts as long as 5000 pulses. There are no apparent obstacles to much higher average powers at higher peak powers.**

I. Introduction

THE generation of microwaves at high power (> 100 MW) has progressed largely on single shot devices. Yet many applications will require repetitive operation at substantial repetition rates [1], implying high average power. Only a few repetitive high power experiments have been conducted. In most the pulse duration is < 50 ns, with average powers less than a kilowatt. Conventional microwave tubes have operated at high average power, but peak power has been low (≪ 100 MW).

The technical challenge of achieving both high peak and high average power is that repetitive operation may 1) evolve material from surfaces which raise the pressure, causing breakdown in the high electric fields (≈ 100 kV/cm) of successive pulses and 2) prevent emission of electron beams from cold cathode surfaces by evaporating monolayers (of gas, oil, water, etc.) and firing again before they can recondense. (It has been suggested that monolayers are the seat of plasma formation from cold cathodes, rather than plasma formation from exploded metal micro projections.) The pressure buildup issue may be addressed by better high vacuum techniques, but only by actually operating at high peak power (> 100 MW) and high repetition rates (> 100 Hz) can the practical limitations be found. Our focus here is on engineering aspects of repetitive HPM systems; a more complete discussion of the CLIA pulser [2] and the experimental results [3], [4] can be found elsewhere.

Manuscript received January 29, 1993; revised March 22, 1993. This work was supported by the Defense Nuclear Agency and the Strategic Defense Initiative Office under a contract managed by the Harry Diamond Laboratory. The RKA bunching section was supplied by NRL under SDIO Contract.

The authors are with the Physics International Company, San Leandro, CA 94577.

IEEE Log Number 9210169.

II. Repetitive Relativistic Magnetron

We modified our *L*-band magnetron [5] for repetitive operation for this experiment. It has six cavities, with cathode, vane and resonator radii of 1.27, 3.18, and 8.26 cm, respectively, and oscillated in the π-mode at 1.1 GHz. This magnetron had produced 3.6 GW when connected to Marx bank/water line drivers.

The modifications for repetitive operation consisted of cooling the anode vanes (via 0.64 cm diameter water channels 0.33 cm from the surface) and the downstream surface where the axial current emitted from the cathode tip is collected. [The maximum power density on the vanes due to the electron beam is ≈ 20 MW/cm^2; for a burst at 250 Hz, the average power density is 300 W/cm^2.] We paid particular attention to creating good electrical contact between parts, for both dc and RF fields, by designing knife edge contacts where possible and by using indium at flat surface contacts, while avoiding virtual leaks. We also used a cryopump for our vacuum system to eliminate possible contamination from backstreaming oil from an oil diffusion pump. Base pressure was 4×10^{-6} torr. Previous single shot experiments have shown that peak power is increased by lowering base pressure [6].

Our initial repetitive operation with the relativistic magnetron revealed some limitations in the operation of the device. Fig. 1(a) shows that as we increased the peak power and repetition rate increasing numbers of the shots "dropped out," i.e., peak power decreased for some of the pulses in a burst. The phenomena seemed random in time, i.e., the peak power did not decrease steadily through a burst of 100 pulses. A histogram of peak power [Fig. 1(b)] shows a drop in the mean of the peak powers as repetition rate increases. Comparing runs at differing peak powers and repetition rates shows that the key parameter is the average electron beam power in the burst. The important variable is not merely the repetition rate, i.e., equivalent conditions seem to occur at roughly equal average powers. It is important to note that these limitations were clearly caused by the interactions within the magnetron; the current pulses from CLIA showed no signs of dropouts.

The dropouts consist of shorter pulses at lower peak power. Even the best pulses are short, and the pulse shape is more triangular than rectangular. For all the pulses the FWHM pulse

0093–3813/93$03.00 © 1993 IEEE

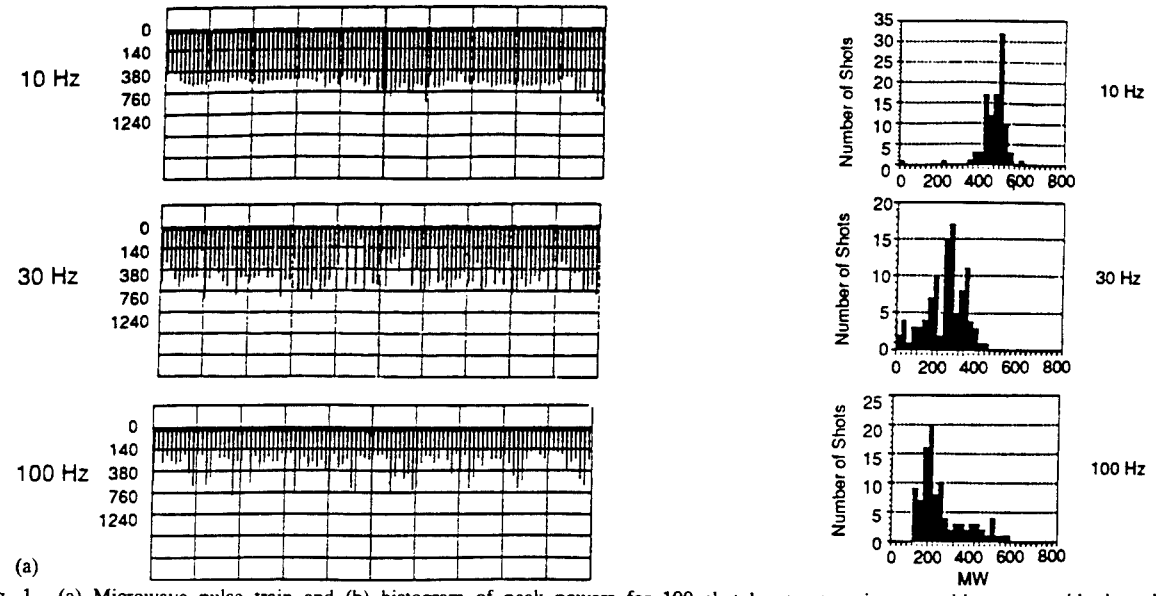

Fig. 1. (a) Microwave pulse train and (b) histogram of peak powers for 100 shot bursts at various repetition rates with the relativistic magnetron before modification. Power levels are in MW.

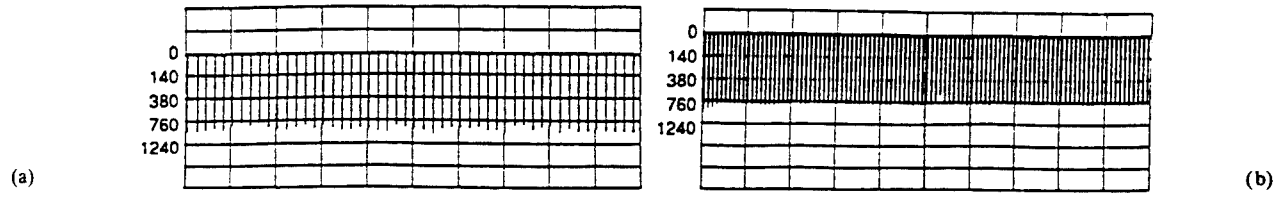

Fig. 2. Microwave pulse train on the magnetron after modification for (a) a 50 shot burst at 100 Hz and (b) a 100 shot burst at 200 Hz. Power levels are in MW.

duration is $\approx$ 30 ns, compared to the 60 ns FWHM of the electrical pulse.

Another observation is that the interval over which dropouts occur is 50–100 ms. Therefore, dropouts at 10 Hz tend to be a single shot but at 100 Hz are typically 5 shots. All of this is consistent with a plasma formation mechanism which, as we will see below, comes from surface contaminants and which prevents high electric fields from existing in the resonator for a period of 50–100 ms. Consequently, our data indicates that the surface contaminants are probably long chain molecules, which could be from the fabrication process, and are not simple absorbed gases such as nitrogen, oxygen, or water vapor.

We undertook a number of simultaneous modifications of the equipment. We made great efforts to remove gassy materials, clean all surfaces by scrubbing with alcohol, and relieve all trapped volumes to eliminate virtual leaks. To remove the worst offenders, we substituted ceramic insulators for the original plastic insulators in CLIA and eliminated the anodizing on the surface of the CLIA stages since both the plastic insulators and anodizing outgas water vapor. We also connected a second vacuum pump and introduced bakeout of the components and limited bakeout of the assembled system. These modifications produced an order-of-magnitude improvement in the base pressure, from the 10^{-5} to 10^{-6} torr range.

After this general cleanup and change in technique we achieved fundamentally more reliable operation. Steady operation at high peak power, with no dropouts, is shown in Fig. 2. After the modifications were made, the FWHM pulse duration increased to $\approx$ 50 ns and the shapes became much more rectangular.

A general observation is that base pressure was not the important variable in achieving high average power provided it was less than 10^{-5} torr. (We intentionally spoiled the vacuum back to the 10^{-5} torr range and observed no detrimental effects.) Bakeout, however, is useful and the continued pulsing of a system gradually improves performance, as in the conditioning process of conventional tubes. Based on the observation that the deterioration of operation was determined by the average power, we now feel that the hierarchy of effects is as follows:

1) The cause of the dropouts is surface contamination; adsorbed materials are not as important. For example, stainless steel and titanium anodes gave equivalent performance even though titanium absorbs water and gases before installation much more strongly than does stainless.
2) Virtual leaks, while they can produce catastrophic breakdown and should be eliminated, are not the cause of the dropout phenomena shown in Fig. 1.
3) Finally, elimination of the ceramic and anodizing was not important in improving performance.

As can seen from Fig. 2, the pulses in the burst are nearly identical, with $\approx$ 1 GW peak and 4.4 kW average powers at 100 Hz. The microwave pulses last as long as the current pulse, i.e., there is no indication of impedance collapse or shifting of the operating point off resonance (effects conjectured to limit

the pulse length in other relativistic magnetron experiments). A significant feature of magnetron operation on CLIA is that the pulse duration of the microwaves (50 ns) is only slightly less than that of the electrical pulse (60 ns). In many previous relativistic magnetron experiments, the ratio is typically 1/3 [7].

The first few pulses are slightly more powerful because there is slightly more current. This is due to the time it takes to establish a steady state within the CLIA power conditioning system. This effect becomes more obvious as the repetition rate is increased, causing a decrease in the peak power even though the average power is still increasing. At 200 Hz the typical peak power dropped to 700 MW while the average power rose to 6.0 kW. At 250 Hz, the trend continued to yield 600 MW peak power and 6.3 kW average power. We tested the system with a 5 shot burst at 1000 Hz (far beyond the average current specification for CLIA) to see if there was a minimum recovery time between pulses. The magnetron operates at 1000 Hz even though CLIA is capable of only a few pulses. Based on the third pulse, we estimate the average power would be $\approx$ 25 kW, with a peak power of 600 MW. Therefore, evolved gas clearing time is less than 1 ms.

III. Repetitive Relativistic Klystron Amplifier

Another microwave source, capable of producing GW power levels in the GHz range, that has seen substantial single-shot development but little repetitive development, is the high-current relativistic klystron amplifier [8]. In our experiment, a 5 kA, 500 kV annular electron beam, 1.8 cm mean radius by 0.2 cm thick, is emitted by a graphite cathode from a foilless diode energized by CLIA. The beam propagates through a two cavity RKA buncher, supplied by M. Friedman and V. Serlin of the Naval Research Laboratory. The drift tube radius is 2.38 cm. A 500 kW L-band magnetron provides the input signal at 1.32 GHz. The input cavity is $3\lambda/4$ long. Radial wires, which are placed at a null at the input frequency and therefore have no effect on it, but load down the fundamental mode, were used originally; they have been removed, as explained below. An axial magnetic guide field, 6–10 kG, is required for beam transport. The current modulation on the beam is measured with a B-dot probe mounted in a section of the drift tube.

Since repetitive operation requires a vacuum system that has a low base pressure before every shot in a burst, one of the main considerations in the design of the RKA is simply good vacuum technique. Copper gaskets are used wherever practical; where the flexibility provided by O-rings is required, viton O-rings are used to allow moderate bake-out ($\approx$ 120 C). Trapped spaces are eliminated by pump-out holes. Good electrical contact between pieces is also required to prevent arcing. As a result, we are able to obtain a base pressure of 1.0×10^{-8} torr.

The electron beam collector used in the single-shot RKA is a flat graphite disk in the drift tube just downstream of the output cavity [8]. For repetitive operation, we instead collect the beam on the inner surface of a 15 cm diameter stainless steel tube, which can be cooled with liquid nitrogen. To make the transition from the drift tube to the collector, a taper was designed that took account of the magnetic field profile and the electron beam parameters. The taper angle was chosen to be large enough to allow the beam to expand along the magnetic field lines without hitting the walls, but not so large that the beam exceeds the local space-charge limited flow condition (by having a radius less than the critical radius), creating a virtual cathode. (The critical radius is proportional to the drift tube radius, with the constant of proportionality determined by the beam energy and current (500 keV and 5 kA).)

Another element of the single-shot design that has proven to be unsuitable for repetitive operation is the use of radial wires in the input cavity for mode selection [8]. During the rising and falling edges of the current pulse, these wires carry the beam return current due to the 20 nH inductance of the remainder of the cavity (10 kV would be generated at the location of the wires at the dI/dt of 5×10^{11} A/s typical of our experiment). The resultant heating causes outgassing, embrittlement, and eventual failure of the wires. The broken wires can then become a source of arcing and breakdown. The net result is that the input microwave signal, as measured in the first cavity, gets progressively shorter during a burst. We have been able to remove the wires without noticeable degradation to the bunched beam.

Fig. 3(a) shows the modulated current on selected shots in a 100 Hz, 100 shot burst at 4.5 kA total current. After some transient behavior in the first $\approx$ 20 shots, the output becomes quite reproducible, with 3.0–3.5 kA modulation. We have successfully increased the number of shots by a factor of ten (to 1000) and the shot rate by a factor of two (to 200 Hz), *simultaneously*, with highly reproducible results [Fig. 3(b)]. The modulated current was 2.0–2.5 kA, out of 3.5 kA total current. The decrease in the modulated current, as compared with 100 Hz operation, is due to the decrease in the cathode voltage, and thus the total current, at the higher repetition rate (since we chose not to increase the CLIA charge voltage for this test) and to a decrease in the efficiency of modulation because the position of the gaps was not optimized for these beam parameters. The data do, however, clearly demonstrate that there are no inherent limitations (at the beam modulation stage, at least) to long bursts of high repetition rate pulses with the RKA.

IV. Discussion

These results extend the envelope of high average and high peak powers for microwave sources. In addition to the points discussed above, what may be most notable about these results are the things that do not limit repetitive operation:

- There is no problem of gas build-up in the magnetron and klystron that could produce impedance collapse or interfere in other ways, though a vacuum system with a base pressure in the low 10^{-6} torr range seems to be required for consistent repetitive operation in the klystron.
- There is no diminution of cold cathode emission after 5000 shots, consistent with the result of Buttram [9] that at least 100 000 shots are required to show diminished emission.

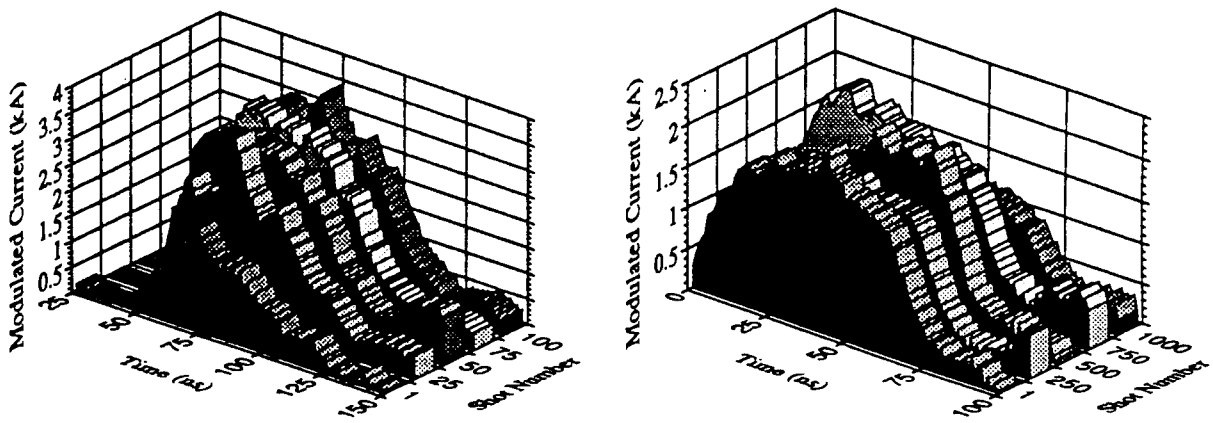

Fig. 3. Amplitude of the modulated current for selected shots in (a) a 100 shot burst taken at 100 Hz and (b) a 1000 shot burst at 200 Hz. The total currents were 4.5 kA and 3.5 kA, respectively.

The results of these experiments allow some general statements about the scaling of HPM sources to high average power. In the L-band magnetron experiments the average power loading is $\approx$ 1 W/cm^2 at 1 Hz. Note that this is the *electrical* power deposited in the surface of the anode. The thermal limitation of conventional microwave sources is $\approx$ 2 kW/cm^2. Therefore, thermal limitations should occur at about 2 kHz in the L-band magnetron. Since the efficiency of relativistic magnetrons is roughly 10%, and the resonator area is about 400 cm^2, the average RF power is limited to $\approx$ 80 kW. At higher frequencies the power limit will be lower: since resonator length and circumference scale with the wavelength, surface area, and therefore the power, will scale as λ^2. Consequently, scaling from the 1.1 GHz L-band magnetron to a 2.8 GHz S-band magnetron will reduce the power limit to $\approx$ 10 kW. For relativistic magnetron systems to achieve higher average powers a number of sources could be phase locked together [10].

On the other hand, relativistic klystrons do not suffer from this limitation because the beam propagates through the bunching structure and is deposited in the collector. The collector can be made arbitrarily large, therefore reducing the average power input to the collector walls. An example of this is a 1 MW average power L-band klystron commercially available from Thomson-CSF [11].

CLIA can be upgraded to extend the pulse length beyond the present capability. Since the microwave pulse lasts as long as the current pulse, there is clearly no impedance collapse and furthermore there must be relative insensitivity to the applied voltage. Thus, there is cause for optimism that these sources would generate longer microwave pulses.

One result of this experiment, that 250 Hz, 100 shot bursts and 1000 Hz, 5 shot bursts can be achieved reproducibly, indicates that much higher average powers should be achievable in the magnetron and other high peak power devices at repetition rates in excess of a kilohertz.

REFERENCES

[1] J. Benford and J. Swegle, *High Power Microwaves*. Boston, MA: Artech House, 1992, ch. 2.

[2] S. Ashby, D. Drury, G. James, P. Sincerny, L. Thompson, and L. Schlitt, "CLIA—A compact linear induction accelerator system," in *Proc. 8th IEEE Intl. Pulsed Power Conf.*, San Diego, CA, 1991, pp. 940–942.

[3] S. Ashby, R. R. Smith, N. Aiello, J. N. Benford, N. Cooksey, D. V. Drury, B. D. Harteneck, J. S. Levine, P. Sincerny, L. Thompson, and L. Schlitt, "High peak and average power with an L-band relativistic magnetron on CLIA," *IEEE Trans. Plasma Sci.*, vol. 20, p. 344 1992.

[4] N. Aiello, J. Benford, N. Cooksey, B. Harteneck, J. Levine, D. Price, R. Smith, D. Sprehn, and M. Willey, "High power microwave generation at high repetition rates," *Proc. Ninth Intl. Conf. in High-Power Particle Beams*, Wash., DC, 1992 (to be published).

[5] R. R. Smith, J. Benford, B. Harteneck, and H. Sze, "Development and test of an L-band magnetron," *IEEE Trans. Plasma Sci.*, vol. 19, p. 628, 1991.

[6] R. Smith, J. Benford, N. Cooksey, N. Aiello, J. Levine, and B. Harteneck, "Operation of an L-band relativistic magnetron at 100 Hz," *Intense Microwave and Particle Beams II*, H. E. Brandt, Ed., *SPIE*, vol. 1407, p. 83, 1991.

[7] J. Benford and J. Swegle, "Crossed-field devices," in *High Power Microwaves*. Boston, MA: Artech House, 1992, ch. 6.

[8] M. Friedman, J. Krall, Y. Y. Lau, and V. Serlin, "Externally modulated intense relativistic electron beams," *J. Appl. Phys.*, vol. 64, p. 3353, 1988.

[9] M. T. Buttram, "Repetitively pulsed electron beam diode lifetime and stability," in *Proc. 2nd IEEE Pulsed Power Conf.* (Lubbock) 1979, p. 61,

[10] J. S. Levine, N. Aiello, J. Benford, and B. Harteneck, "Design and operation of a module of phase-locked relativistic magnetrons," *J. Appl. Phys.*, vol. 70, p. 2838, 1991.

[11] "Microwave tubes and devices," Catalog DTE 082, Thomson-CSF, 106 (1986).

James N. Benford (SM'91) received the M.S. and Ph.D. degrees in physics from the University of California, San Diego and the B.S. degree in physics from the University of Oklahoma.

He is the Director of the High Power Microwave Division at Physics International Company, Olin Corporation, San Leandro, CA. He has been conducting research in the field of high-power microwaves for the last 10 years. Over the last 22 years at Physics International, he has also been the Technical Director and Program Manager of many major experimental programs in high-power microwaves, electron-beam fusion research, and beam-propagation physics. He has also been involved in system analysis and design programs on linear-induction accelerators, pulsed-power generators, beam and plasma experiments, fusion reactor studies, and other pulsed power research. He has over 25 publications in scientific journals and proceedings in the field of high-power microwave. He is co-author of *High Power Microwaves* (Artech House, 1992).

Nicholas J. Cooksey received the B.S. degree from Montana State University in 1988.

Since he joined Physics International Company, Olin Corporation, he has worked on a variety of high-power microwave projects, including vircators, phase-locked and repetitively-pulsed magnetrons, and klystrons.

Jerrold S. Levine received the Ph.D degree in applied physics from Stanford University, Stanford, CA, in 1981.

After working in the fields of gyrotron development and electron cyclotron heating of tokamak plasma, he joined Physics International Company, Olin Corporation, in 1984. He has worked there on projects in radiation simulation using bremmstrahlung and Z-pinch sources, pulsed-power design, inductive energy store/fast opening switches, and X-ray lasers. His recent concentration on high power microwave sources involves phase-locked arrays of relativistic magnetrons and repetitively-pulsed, high-current relativistic klystron amplifiers.

Richard R. Smith, photograph and biography not available at the time of publication.

Design and operation of a module of phase-locked relativistic magnetrons

J. S. Levine, N. Aiello, J. Benford, and B. Harteneck
Physics International Company, 2700 Merced Street, San Leandro, California 94577

(Received 11 March 1991; accepted for publication 6 June 1991)

We have achieved phase-locked operation of a module consisting of up to seven relativistic magnetrons. The magnetrons are connected by waveguide in a peer/peer configuration, with no one magnetron acting as a master oscillator. The signals used for coupling are each a substantial fraction of a magnetron's radiated power. Total extracted power, at 2.8 GHz, was 2.0 GW with four magnetrons and 2.9 GW with seven. Several interconnection geometries were explored. One particular geometry was found to produce qualitatively better phase-locked operation than any other. This was in agreement with the predictions of a numerical model of the magnetrons as coupled van der Pol oscillators.

I. INTRODUCTION

There is continuing interest in steerable antenna arrays producing >100 GW of power in the GHz frequency range.[1] There are two ways to efficiently energize such an array: build sources of ever increasing power, or combine the outputs of multiple phase-coherent sources. The first approach is limited by electric field breakdown within microwave cavities and mode competition that occurs in large, overmoded cavities. We have therefore pursued the second approach.

In order to combine the outputs of multiple high-power microwave sources in a steerable antenna array, the sources must be at the same frequency with a known phase difference between them. Only then is it possible to produce a controllable beam using constructive interference in the far field of the antenna. It is important to note that the *absolute* phase differences at the sources are not particularly important, since they can be corrected for in the transmission system between the sources and the antenna. The critical criteria are that the relative phases must be *constant* during each pulse and *reproducible* pulse-to-pulse. It is this requirement of reproducibility that distinguishes frequency locking, observable on a single pulse, from phase locking.

The interactions between sources that produce phase locking can be distinguished as master/slave or peer/peer and as weak or strong coupling. The first distinction reflects whether one source operates independently of the others, controlling their phases, or whether all the sources adjust to each other. The second distinction reflects the ratio of the signal injected into a source for phase locking to the signal naturally occurring in that source. For weak coupling this ratio is much less than unity; for strong coupling it is of order unity. (It is possible to overdrive an oscillator, with the ratio exceeding unity, but that is inefficient and may lead to stability problems).[2]

While it is clearly desirable to operate in the weak coupling régime, i.e., to control a powerful signal with a weak one, there is a major drawback within the realm of ultrahigh-power relativistic microwave oscillators: locking time. Since the locking time scales inversely with the coupling[3] and these sources have typical pulse lengths of only ≈ 50 ns, strong coupling is desired.

There have been several recent experiments investigating phase locking of magnetrons and vircators in both master/slave and peer/peer configurations. A series of experiments, in which all the sources are energized by a single pulsed-power generator, have demonstrated phase locking of: two relativistic magnetrons in peer/peer configuration,[4] a vircator by a magnetron in a master/slave configuration,[5] two vircators as peers,[6] and two vircators, either disconnected from each other or connected as peers, by a master magnetron.[7] In all the peer/peer experiments, a waveguide bridge between the oscillators provided the coupling; a plunger in the bridge allowed comparison of connected and unconnected operation on a shot-to-shot basis. In addition to phase locking, it was also noted that the coupling improved the simultaneity of oscillations, an important added bonus. In the master/slave experiments, the magnetron was the master oscillator by virtue of a long waveguide between the magnetron and the vircators and the timing of the oscillations within each source. The magnetron oscillated first, at lower current, and its signal was delayed until the vircators were ready to oscillate. By the time the vircator signal could propagate back to the magnetron, it was no longer oscillating.

Frequency locking has also been demonstrated in an experiment with two separate pulsed-power generators, connected to two independent cathodes, creating two vircators in a common anode cavity.[8] The flexibility of two drivers allowed the relative timing of the two vircators to be varied. It was found that prefilling of the cavity by one vircator was necessary for the two to frequency lock. This is a clear distinction from the former results where phase locking was observed between vircators in separate cavities with no prefilling.

To expand upon this work, we have designed and built a compact module of relativistic magnetrons, in both "half module" and "full module" configurations. Communication between any two magnetrons is obtained by connecting short sections (half wavelength) of waveguide between the back of a resonator on each, coupled through an iris. The power used for coupling is a significant fraction of the

 0021-8979/91/052838-11$03.00

total produced, so we are clearly in the strong coupling régime. By choosing which magnetrons to connect together, we can investigate several different interconnection geometries.

II. NUMERICAL MODELING

A. Derivation of model equations

Woo *et al.*[9] have modelled the interaction of two mutually coupled magnetrons by a coupled van der Pol equation,[10] leading to the same equations for phase and amplitude evolution as result from an equivalent circuit analysis. For the present work, we need to extend the model to include the interactions of multiple magnetrons. We do this by summing over coupling terms (using the notation of Ref. 9)

$$\frac{d\phi_i(t)}{dt}=\omega_{0i}-\sum_{j\neq i}\frac{\omega_{0i}\rho_{ij}(t)}{Q_i}\sin[\phi_i(t)-\phi_j(t-\tau_{p,ij})], \tag{1}$$

where ϕ_i, ω_{0i}, and Q_i are the instantaneous phase, natural frequency, and quality factor of the ith magnetron, ρ_{ij} and $\tau_{p,ij}$ are the coupling constant and phase velocity transit time between the ith and jth magnetrons. The coupling constant is the ratio of the injected electric field, E_{0j}, from magnetron j, to the existing electric field in magnetron i, E_{0i}, i.e.,

$$\rho_{ij}\equiv\frac{\hat{E}_{0j}}{E_{0i}}=\left[\frac{\hat{P}_{0j}}{P_{0i}}\right]^{0.5}, \tag{2}$$

where the P's are the incoming and outgoing powers of the magnetrons and the circumflex represents delay due to the group velocity transit time, $\tau_{g,ij}$.

Frequency locking is achieved when the phase difference between the magnetrons becomes constant, after some transient, when Eq. (1) is integrated for any particular initial phases. Phase locking has the added requirement that the constant phase differences be independent of the initial phases. In the two magnetron case, the phase difference is[9]

$$\Delta\phi=\sin^{-1}\left(\frac{\Delta\omega_0 Q}{2\omega_0\rho\cos\phi_c}\right), \tag{3}$$

where $\omega_0=(\omega_{01}+\omega_{02})/2$, $\Delta\omega_0=\omega_{01}-\omega_{02}$, and ϕ_c is the phase shift across the coupler. For a solution to Eq. (3) to exist, the absolute value of the argument of the arc sine must be <1, showing the interrelationships between the fractional frequency mismatch, $\Delta\omega_0/\omega_0$, the quality factor, the coupling strength, and the connector length:

$$\rho>\left|\frac{Q\Delta\omega_0}{2\omega_0\cos\phi_c}\right|, \tag{4}$$

which can be seen as a modified Adler[3] relation.

B. Application to magnetron module

In using Eq. (1) for modeling the magnetron module, we first of all must determine the coupling coefficients,

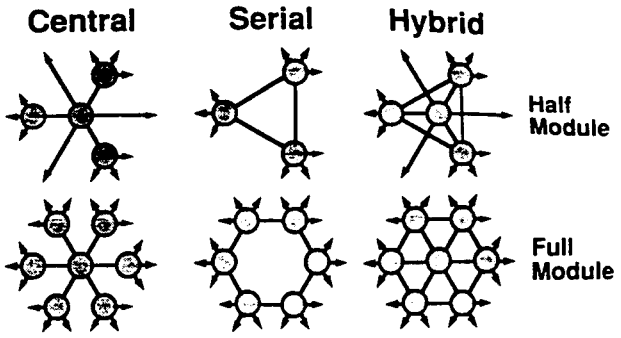

FIG. 1. Interconnection geometries. Lines are connectors between resonators on magnetrons, which are shown as circles. Arrows are power extraction ports from other resonators.

which reflect the interconnection scheme. The basic schemes are shown schematically in Fig. 1. The magnetrons used in the experiment are of the basic A6 design,[11] with six resonators, allowing a maximum of six connections for coupling and/or power extraction, referred to collectively as "open resonators." A waveguide bridge between the magnetrons, coupled through irises, provides the connection. Therefore, from the geometry, we deduce

$$\rho_{ij}(t)=\left[\frac{P_j(t-\tau_{g,ij})}{P_i(t)}\frac{1}{n_j}\right]^{0.5}, \tag{5}$$

where n_j is the number of open resonators on magnetron j.

We have simplified our integration of Eq. (1) in two ways. Rather than solve the amplitude equation for the coupled system to self-consistently determine the power levels,[9] and thus ρ, we assume (based on experimental observation) that each magnetron has the same pulse shape, either triangular or rectangular. ρ is thus completely determined by the geometry and assumed pulse shape. Since the coupling coefficients depend on the ratio of powers, this represents only a small correction. We have further simplified the numerical bookkeeping by using $\tau_{p,ij}$ instead of $\tau_{g,ij}$ in the computations.

Based on the two-magnetron analysis,[9] the optimal length for the connectors should be some multiple of a half-wavelength, as can be seen from Eq. (4). For even multiples, the stable phase difference should be $\approx 0°$, for odd multiples, $\approx 180°$.

There is also a closure condition that requires that any closed loop, across connectors and resonator-to-resonator within magnetrons, has no net phase shift. Since we anticipate magnetron operation in the π mode, in which adjacent resonators are 180° out-of-phase, the hybrid connection in the half module requires integral wavelength connectors between the peripheral magnetrons, and the full module requires half-integral wavelength connectors. Since we had a design goal of a "compact" module, our first choice was a connector length of one-half wavelength.

We have performed a systematic study to determine the optimal geometry for phase locking. The variables that were exercised in the analysis for each of the configurations of Fig. 1 were the connector lengths, the spread of the

individual resonant frequencies (the ω_0's), and the Q's (assumed to be the same for all the magnetrons).

We examined the effect of frequency spread by randomly assigning the ω_0's within a band about a center frequency: 20–70 MHz about 2.8 GHz. The standard deviation of the chosen frequencies, σ_f, was then calculated to represent the true measure of the frequency spread. We set the Q values for all the magnetrons to be the same, and let them range from 20 to 50.

To distinguish true phase locking from frequency locking, we assigned three sets of randomly chosen initial phases for the magnetrons as the starting point for integrating Eq. (1). The phase difference of each magnetron, relative to a reference magnetron, should then evolve to a constant, reproducible, value. The larger the frequency spread and Q value, and the larger the range of connector lengths about the design value, for which this will happen, the "better" the geometrical configuration.

Wave forms for full module cases that phase lock and do not phase lock are shown in Figs. 2(a) and 2(b), respectively. The differences are the Q's and the geometries ($Q=20$, hybrid for the locked case and $Q=50$, central for the unlocked case). The locked case shows all the anticipated behavior: regardless of initial phase, each magnetron rapidly evolves to a constant phase relative to the reference magnetron, that phase being near 0° or 180°, depending on which resonator the magnetron is connected to. The unlocked case shows no such reproducibility; indeed the relative phases of some magnetrons vary monotonically throughout the pulse, demonstrating a lack of even frequency locking.

As a figure-of-merit for phase locking, we have defined a "normalized power density," S, and an efficiency, η, as

$$S(t)=\left(\sum_{j}^{N}\cos[\phi_j(t)-\phi_n(t)-\delta\phi_j]\right)^2 + \left(\sum_{j}^{N}\sin[\phi_j(t)-\phi_n(t)-\delta\phi_j]\right)^2, \tag{6}$$

$$\eta=\frac{\int P(t)S(t)dt}{N^2\int P(t)dt}, \tag{7}$$

where the sum is over the magnetrons from which power is actually extracted (see Fig. 1), and $\delta\phi_j$ is an external phase correction, such as would be made by differing waveguide lengths between the magnetrons and antennas or by the use of phase shifters, and magnetron n is the reference magnetron. To determine the external phase corrections, we use the final phase differences from the computer run with the first set of initial phases to correct the subsequent two sets. The calculated efficiency is then based on only these last two sets. $S(t)$ represents the power density that could be placed on a target by an antenna array; η normalizes that to the maximum possible with a completely coherent source. In Eq. (7), $P(t)$ is the power pulse shape and the integral is taken over the entire pulse length.

In analyzing the results, we find that neither Q nor σ_f individually control trends, but that their product does. This is a reasonable result, since Q determines the width of the resonance in each magnetron, and σ_f reflects how far each magnetron must shift in frequency to come to a common frequency. Looking at Eqs. (3) and (4), this could have been anticipated.

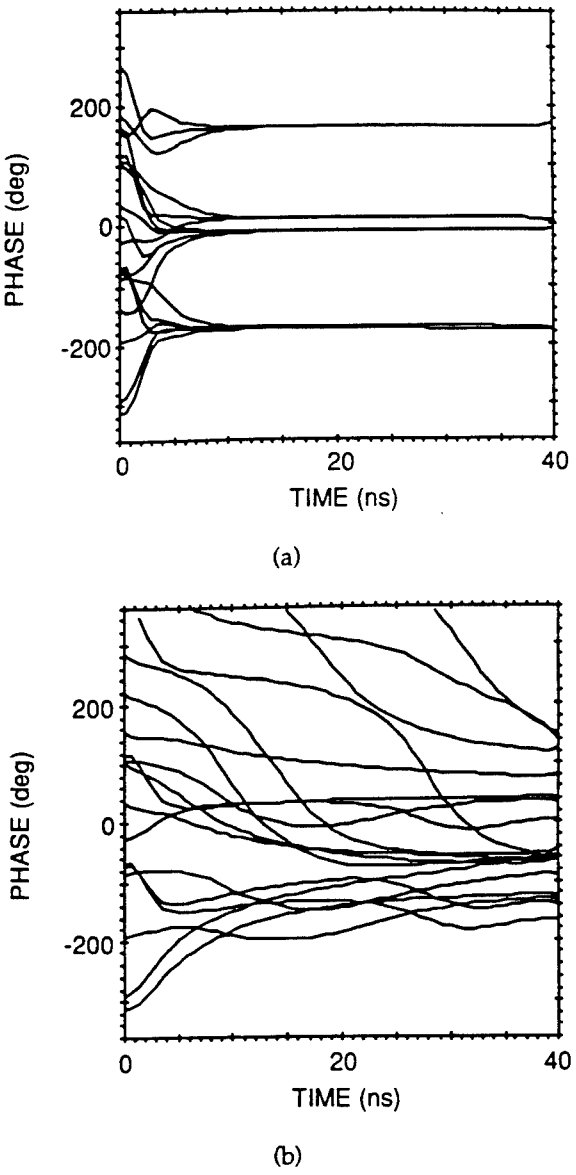

FIG. 2. (a) Evolution of the phase difference of six magnetrons relative to the seventh for a case that phase locks. Three sets of randomly assigned initial phases produce the same final relative phases. (b) The same frequencies and initial phases, but under conditions that do not phase lock. The final phases are always mapped to ±180°, producing the appearance of a larger spread in the initial phases in (b).

A comparison of the three configurations of the full module, for connectors one-half wavelength long, is shown in Fig. 3. The hybrid configuration is clearly preferable. We hypothesize that this is due to the greater "connectedness" of the hybrid configuration: each peripheral magnetron is being driven by three other magnetrons, the central magnetron by six others. No magnetron can get very far "out of line" before it is pulled back "into line." The serial configuration shows some poor efficiency operation even at

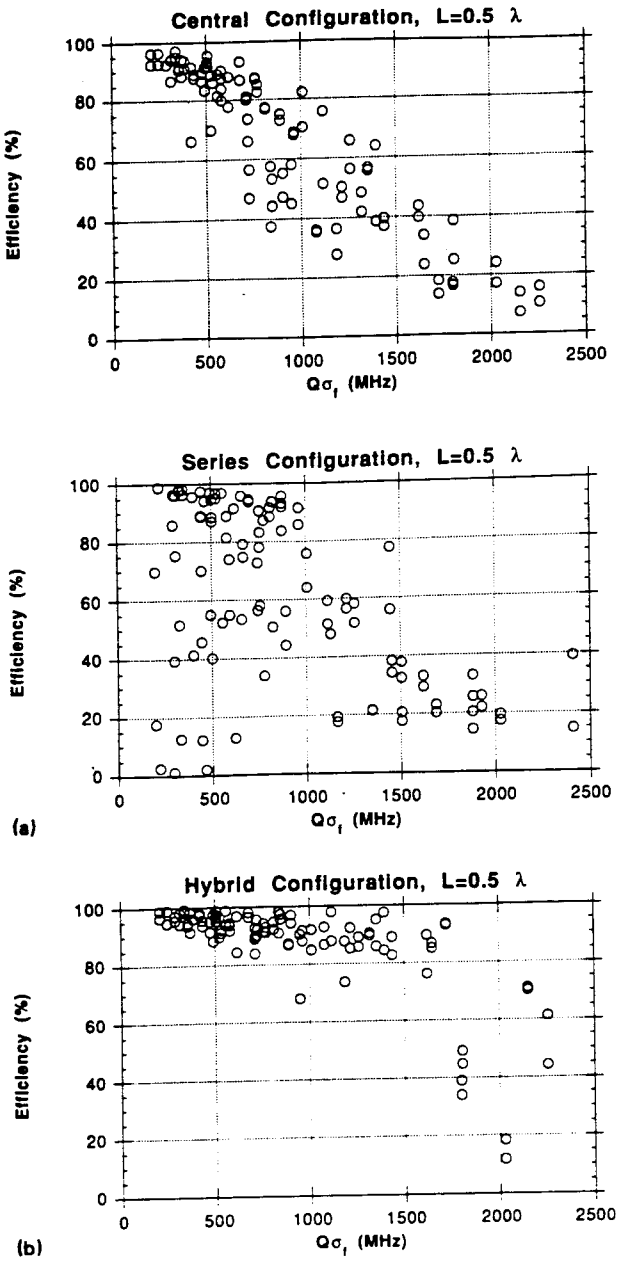

FIG. 3. Comparison of radiation efficiency in the central, serial, and hybrid configurations of the full module for one-half wavelength connectors.

low $Q\sigma_f$. This is because there can be multiple stable states of the array, with additional multiples of 60° phase shifts between magnetrons. The external phase corrections deduced from the first run therefore may be inappropriate for subsequent runs as the module shifts between states from one run to the next.

We find that the efficiency is fairly independent of the connector length, so long as it is some integral number of half wavelengths, from one to five half wavelengths. In Fig. 4, we calculated for only odd numbers of half wavelengths due to the selection rule for the hybrid geometry. (Certainly, once the transit time through the connectors is comparable to the pulse length, efficiency would become connector length dependent.)

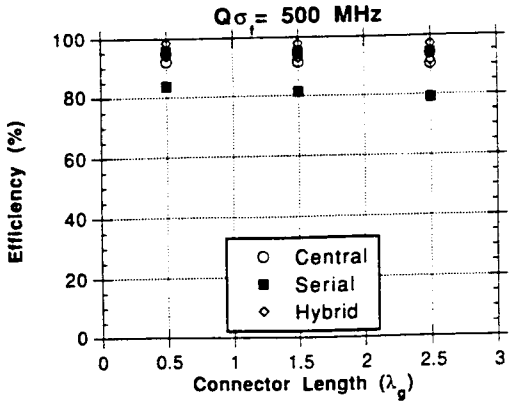

FIG. 4. For connectors short relative to the pulse length, efficiency is independent of length, so long as some integral number of half wavelengths is used. The hybrid selection rules preclude phase locking with an integral number of wavelengths.

As a practical matter, it is important that the module be able to phase lock, even if the connectors are not exactly an integral number of half wavelengths. This reflects some uncertainty about the exact frequency at which phase locking will occur, and thus the phase shift across a given length of waveguide, and the manufacturing tolerance for the hardware. Since the length of the connectors, in waveguide wavelengths is $L_w = L/\lambda_g$, where L is the length and

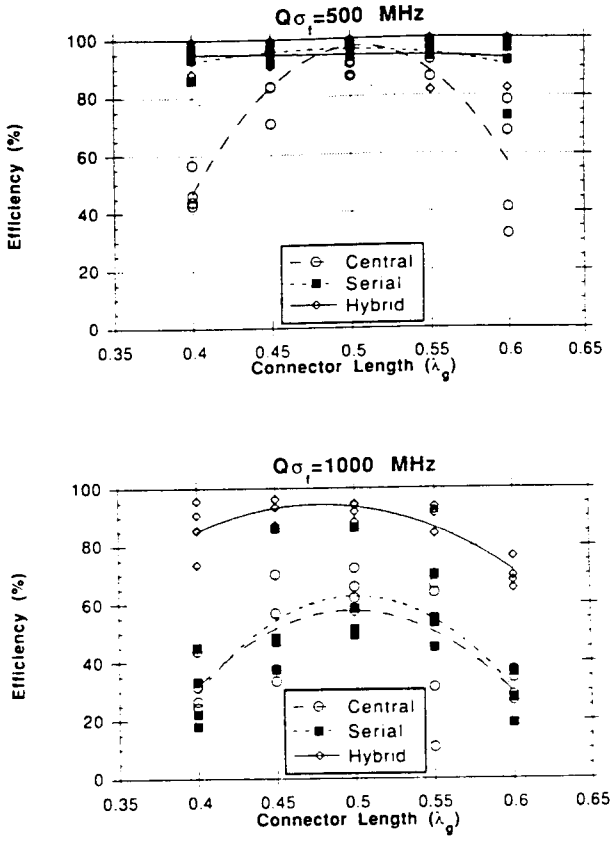

FIG. 5. Efficiency for the three configurations at two values of $Q\sigma_f$ as a function of connector length. The lines are quadratic least-squares fits, drawn as visual aids.

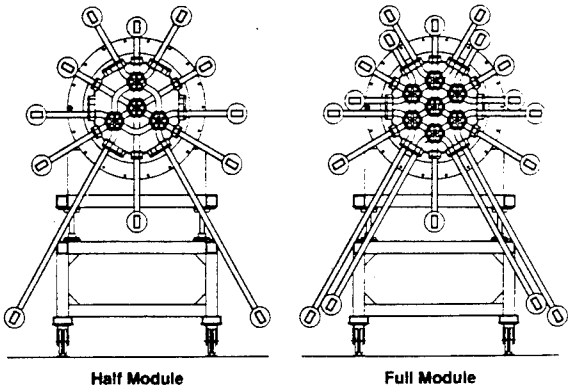

FIG. 6. Half and full module versions of the magnetron module. As shown, the interconnecting waveguide is configured for the hybrid geometry in both versions.

λ_g is the wavelength in the connecting waveguide, the fractional deviation from the design value is

$$\frac{\Delta L_w}{L_{w0}}=\frac{\Delta L}{L_0}+\frac{f_0\Delta f}{f_0^2-f_c^2}, \tag{8}$$

where the subscript 0 refers to design values and f_c is the cutoff frequency in the waveguide. With our design parameters [L_{w0} = 0.5 wavelengths, f_0 = 2.8 GHz, L_0 = 8 cm, f_c = 2.08 GHz (WR280 waveguide)], a worst case of ΔL=0.5 cm and Δf=0.1 GHz, produces ΔL_w = 0.07 wavelengths. As shown in Fig. 5 for two cases of $Q\sigma_f$ (500 and 1000 MHz), the hybrid configuration is fairly insensitive to connector length variations as large as $0.1\lambda_g$. The serial configuration is also tolerant of connector length inaccuracy at the lower value of $Q\sigma_f$, but not at the higher value, where it is inefficient anyway. The central configuration is the most sensitive of all.

III. EXPERIMENTAL PROCEDURE

A. Design of hardware

The magnetron module was designed to operate in both the half and full module configurations, as shown in Fig. 6. The cathodes are 0.5-cm radius stainless-steel cylinders, extending through the anode blocks, connected to a common bus plate, which is attached to the Physics International CAMEL-X pulser (1 MV, 2.8 Ω, 65 ns nominal

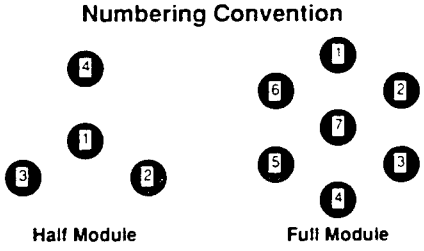

FIG. 7. Numbering convention used in this paper for the half and full module.

parameters). The anodes are of the A6 design, 7.2-cm long, with inner radius of 2.1 cm. There are six resonators of radius 4.2 cm, each subtending 20°. Endcaps of 2.1-cm inner radius close off both ends of the resonators. There is a single vacuum vessel, containing all of the magnetrons and interconnecting waveguides. The magnetic field is produced by a single external Helmholtz coil set, producing up to 9.5 kG with a 300-kJ pulsed capacitor bank.

Eighteen penetrations in the vacuum vessel allow power extraction and diagnostic access. Note that for the full module, there is no extraction from the central magnetron. The microwaves are absorbed in waveguide dummy loads, all in vacuum, connected to the ends of the waveguide arms shown in Fig. 6.

All of the interconnecting waveguides can be removed, and the extraction irises blanked off, allowing us to configure the module in the various interconnection geometries. The numbering convention of the magnetrons is shown in Fig. 7.

B. Diagnostics

The electrical diagnostics for the system consist of a voltage monitor on the CAMEL-X marx, two total current Rogowski coils, and individual Rogowski coils on the input to each magnetron. All the signals are collected on a digital data acquisition system, facilitating inductive correction of the voltage from the marx to the magnetrons and comparison of the total current measurements with the sum of the individual current measurements, indicating breakdown in the electrical feed.

One waveguide arm from each magnetron contained a power sampler, with approximately 65–70 db coupling. Each signal was divided several times for simultaneous measurement with a crystal detector for power and pulse shape determination, a heterodyne receiver for frequency determination, and a phase discriminator for the relative phase measurement.[12] One of the magnetrons, typically the #1 magnetron in Fig. 7, served as the reference against which all the other phases were measured.

Like the electrical diagnostics, all the microwave diagnostics were recorded with the digital data acquisition system. The bandwidth of the system was ≈400 MHz, which provided adequate response for most of the measurements. The limitation arose in the heterodyne signal; if the microwaves were more than 400 MHz away from the local oscillator, they disappeared from the heterodyne signal. (The signature of such a large frequency difference was that the crystal detector pulse was much longer than the heterodyne signal.) We calibrated each of the crystal detectors, and fit the curves with either an exponential or quadratic function to automatically calculate power pulse shapes from the measured signals.

The phase discriminators have four outputs: V1, V2, V3, and V4. The differences, in pairs, give the cosine and sine of the relative angle between the signals, ϕ, with an amplitude determined by the product of the signal amplitudes, A and B:

$$V1 - V2 = AB\cos\phi,$$

$$V3 - V4 = AB\sin\phi. \tag{9}$$

The differences are constructed by analog methods, with high-frequency pulse transformers, and then recorded. When taking the ratio and the arc tangent, we determine the quadrant of the relative angle by checking the polarity of the cosine and sine terms. The range of the display is chosen for the least confusing output, sometimes $-180°$–$180°$, sometimes $0°$ to $360°$, etc. Before and after the microwave pulse, both signals are just noise producing wild variations in the processed wave forms. Therefore the results are meaningful only during the actual microwave pulse, i.e., the smoothly varying part of the signal.

C. Experimental results

1. Half module

Most of our work was with the central configuration (see Fig. 1). Some attempts with the hybrid configuration were made, but breakdown problems in the waveguides extracting power from the central magnetron made this

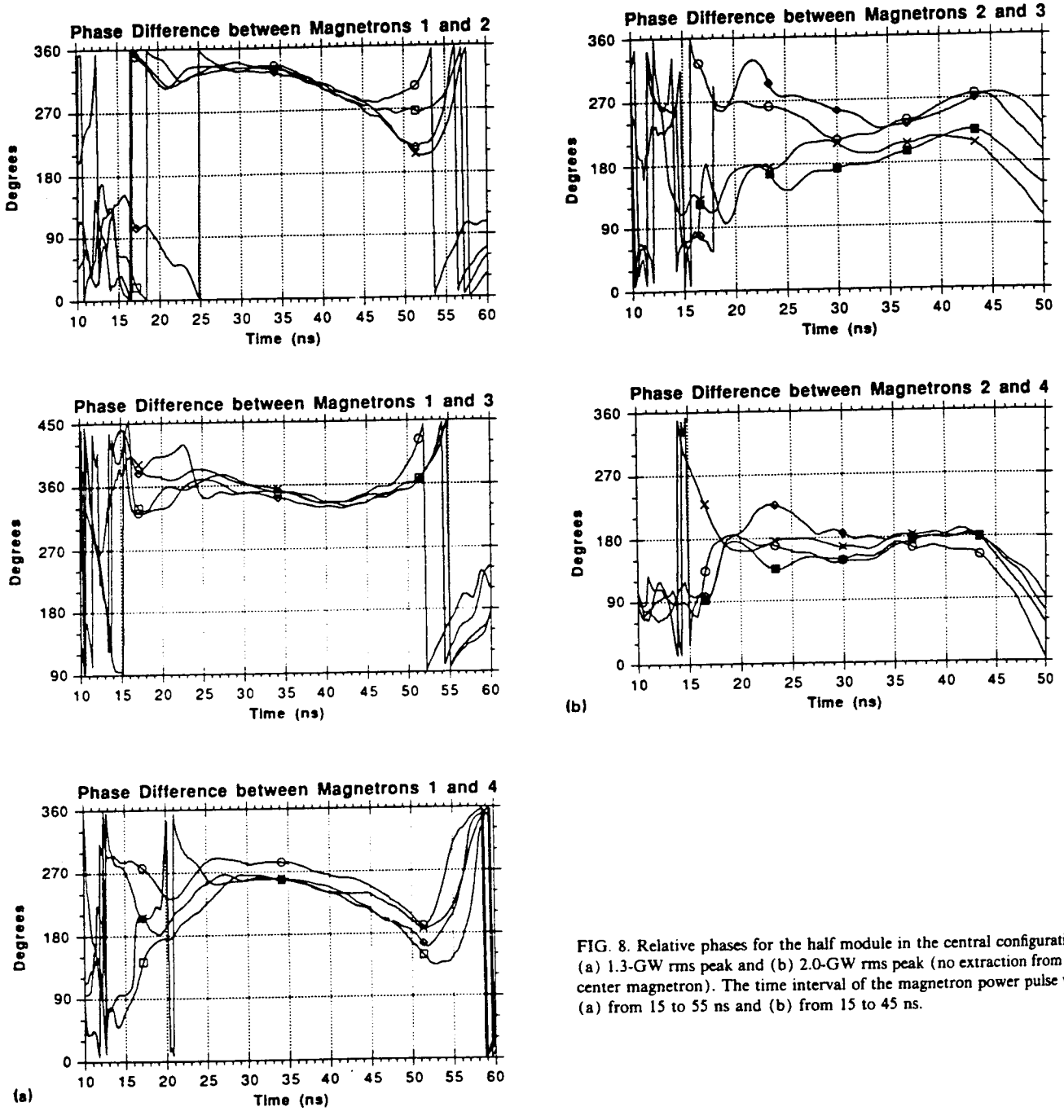

FIG. 8. Relative phases for the half module in the central configuration: (a) 1.3-GW rms peak and (b) 2.0-GW rms peak (no extraction from the center magnetron). The time interval of the magnetron power pulse was (a) from 15 to 55 ns and (b) from 15 to 45 ns.

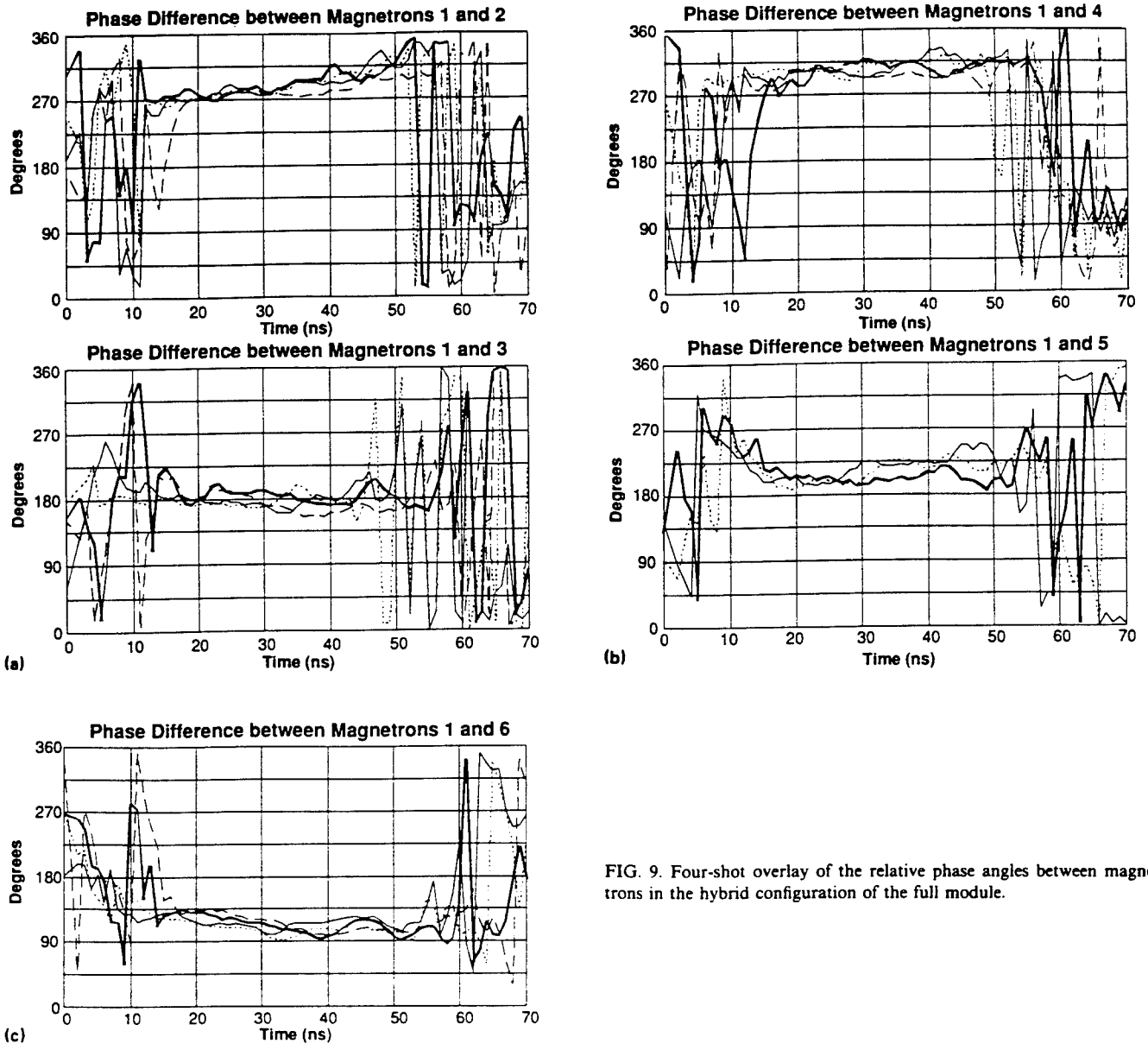

FIG. 9. Four-shot overlay of the relative phase angles between magnetrons in the hybrid configuration of the full module.

mode unreliable. In unconnected operation, the frequency was 2.8 GHz, with a spread of <30 MHz between all the magnetrons.

Four-shot overlays of phase discriminator measurements for two power levels of centrally connected operation are shown below in Fig. 8. It takes, typically, 5 ns from the onset of microwave output for the phases to lock (the zero of time in the graphs is related to the starting of the data acquisition system and not the microwaves). The phase locking is then maintained for the duration of the power pulse. The phase difference between magnetrons 1 and 3 in Fig. 8(a) demonstrates "perfect" phase locking: the relative phase is constant during the entire power pulse and reproducible shot-to-shot. The remaining lower power data shows excellent reproducibility, but some phase drift during each shot. The higher power data shows only slightly reduced shot-to-shot reproducibility with comparable phase drift. These two aspects of phase locking have essentially the same implication for an antenna array: the $\pm 22.5°$ band in phase in the lower power shots would degrade the power density in the far field by no more than 10% from the maximum possible, the $\pm 30°$ band in the higher power data would degrade the power density by no more than 15%.

2. Full module

The magnetron module was designed, from the outset, to accommodate an upgrade to the full, seven-magnetron configuration (see Fig. 6) with a minimum of modification. One significant difference was that the central magnetron (when present) was connected to the six peripheral magnetrons so that there was no diagnostic access.

Phase locking in the hybrid configuration: Based on our numerical modeling of the magnetron module, we anticipated that the hybrid configuration had the best chance of phase locking. We therefore began our experiments in the hybrid mode.

Figure 9 is an overlay of the relative phase measurements for four consecutive shots; the power measured for

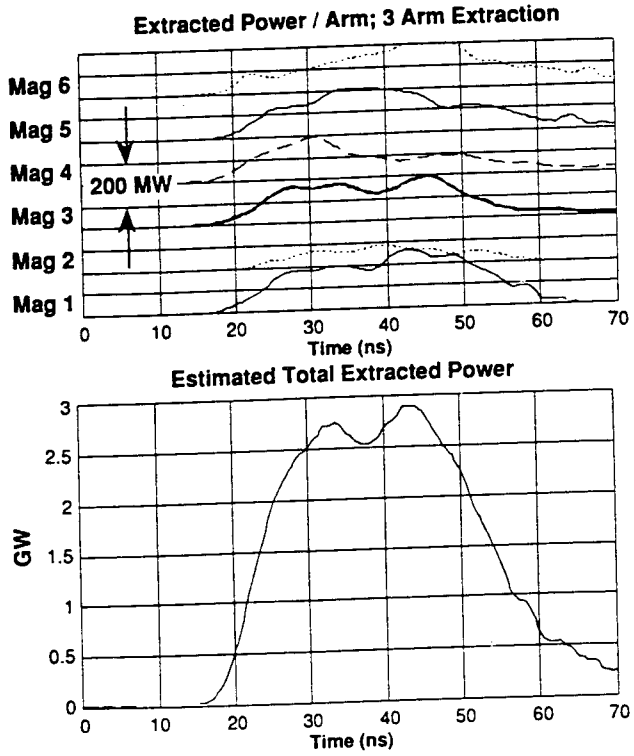

FIG. 10. Output power for the third shot of the sequence in Fig. 9.

one of the shots (the third in the sequence) is shown in Fig. 10. The total power is "estimated" in that we have assumed that the three extraction arms on each magnetron have the same power (supported by previous measurements). We thus sum the measured powers and multiply by three. [N.B., this is an upper bound on the S function defined in Eq. (6) since there is no correction for the relative phases. When phase locking is successful, they are equivalent; when phase locking is unsuccessful, the estimated power is larger than S.]

This data clearly demonstrates successful phase locking. It takes, at most, 5 ns for the phases to come together, as measured from the beginning of the power pulse. (As above, the zero reference time is related to the data acquisition system and not to the microwaves.) The small drift in the phases of magnetrons 2 and 6, relative to 1, would account for no more than a 5% degradation of the total possible power delivered from an antenna tuned for the center of the pulse. The shot-to-shot reproducibility is within the noise variation of each shot. This is amazingly good phase locking, qualitatively better than that observed in the half module experiments or the previously reported dual-magnetron experiments.[4] In the course of the experiment, the hardware was disassembled and reassembled several times; it was always possible to obtain comparable results quickly.

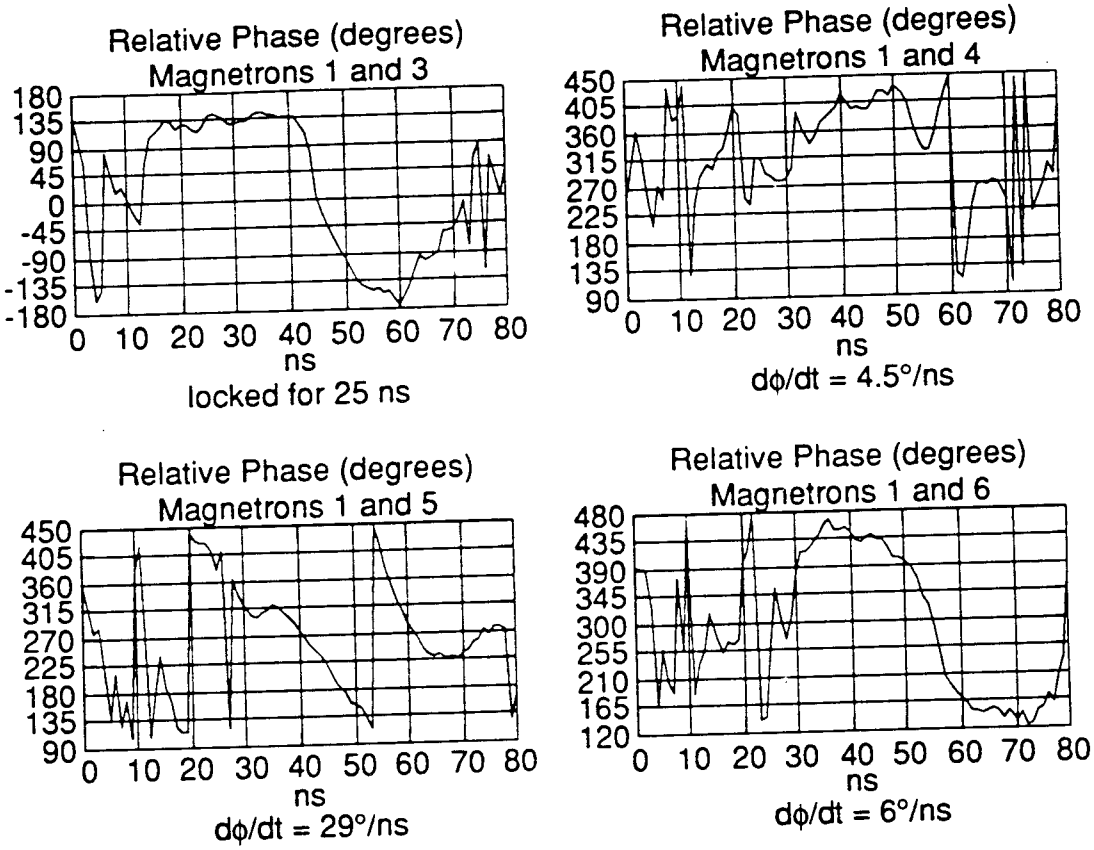

FIG. 11. Relative phase measurements for a single shot in the central geometry. The shot-to-shot reproducibility was so poor that an overlay would only obscure the results. (No data were taken from magnetron 2 for this shot.)

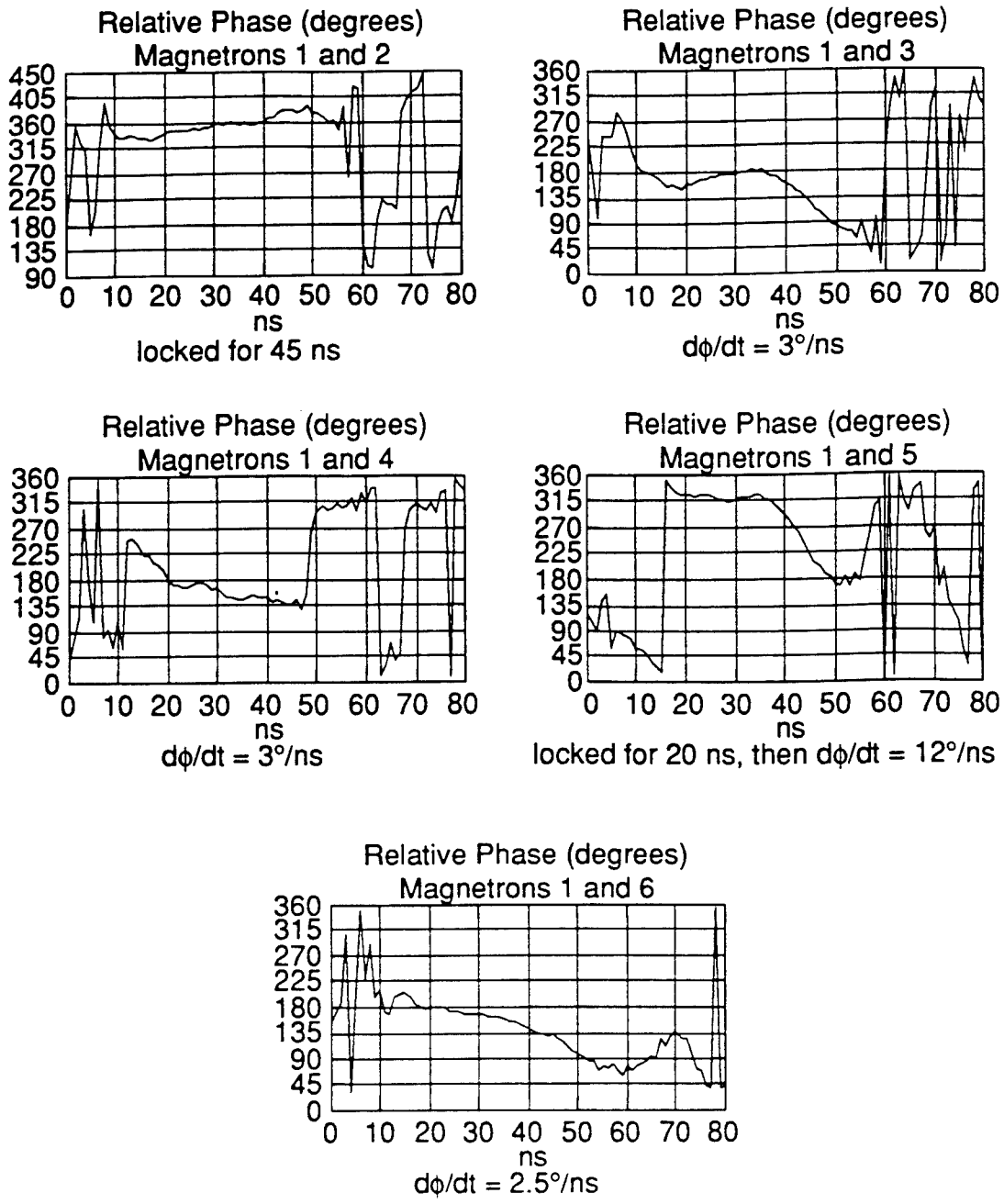

FIG. 12. Relative phase measurements for a single shot in the serial geometry. The shot-to-shot reproducibility was so poor that an overlay would only obscure the results.

Investigation of other interconnection geometries. Figures 11, 12, and 13 are relative phase measurements for the central and serial configurations of Fig. 1, and a linear chain (the serial configuration with the connection between magnetrons 3 and 4 removed), respectively. The estimated total power levels for these shots were all 1.5–2.0 GW. We see in these shots various types of phase evolution, none of which matches the phase locking of the hybrid mode. There are magnetrons that show a steady, rapid increase in their phase difference (e.g., magnetrons 1 and 5 in the central geometry and magnetrons 1 and 3 in the linear chain). The explanation is that these are magnetrons operating at different frequencies (with frequency differences of 81 and 33 MHz, respectively). There are also cases where the frequency differences are small enough that the relative phases are constant, or nearly constant, for a substantial portion of the pulse. However, even in these cases, the lack of shot-to-shot reproducibility (e.g., see the relative phase of magnetrons 1 and 4 and the relative phase of magnetrons 1 and 5 in the linear chain) make these unsuitable for a phased-array antenna. This is the distinction between frequency locking and phase locking. (These sources could conceivably create a microwave beam, but it would be useless since the direction in which the beam pointed would vary on a shot-to-shot basis.)

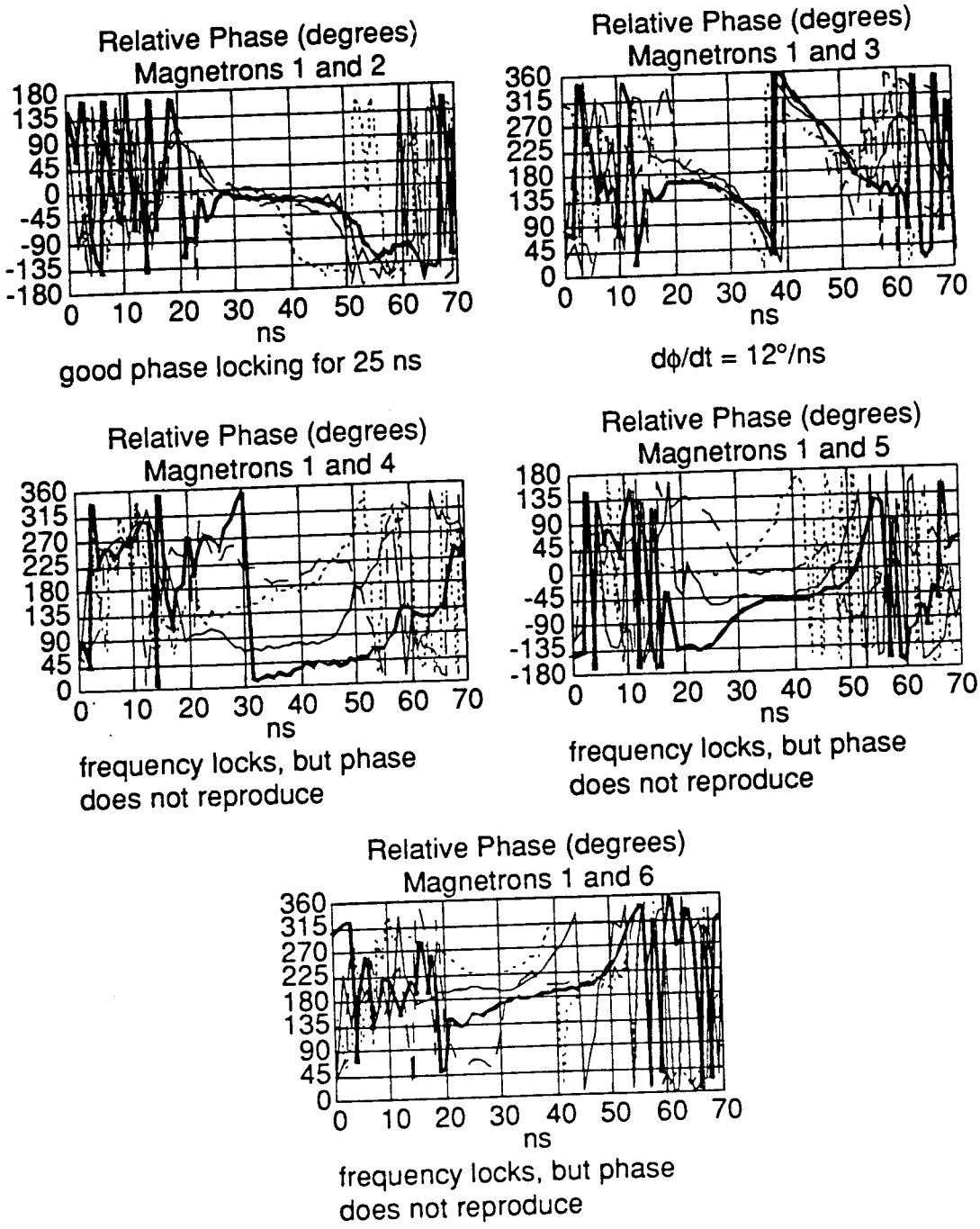

FIG. 13. Relative phase measurements for an overlay of four shots in the linear chain geometry.

IV. SUMMARY

Figure 14 qualitatively summarizes our present and previous[4] observations on geometries that support phase locking. The first column shows that the phase locking in a linear chain geometry degrades as the number of magnetrons increases. Connecting the ends of the chain in the six-magnetron serial geometry does not reverse the trend. The second column shows that the same is true of the central configuration: it phase locks for the half module but not the full module. The hybrid configuration of the full module, as shown in the last column, phase locks very well. One generalization supported by the data is that more connection between magnetrons produces better phase locking.

There are two approaches to further increase the power from phase-locked magnetrons. The first is to add another ring of magnetrons around the existing seven to create a module of 19 magnetrons. This has an efficiency drawback since one could extract power from only twelve of them.

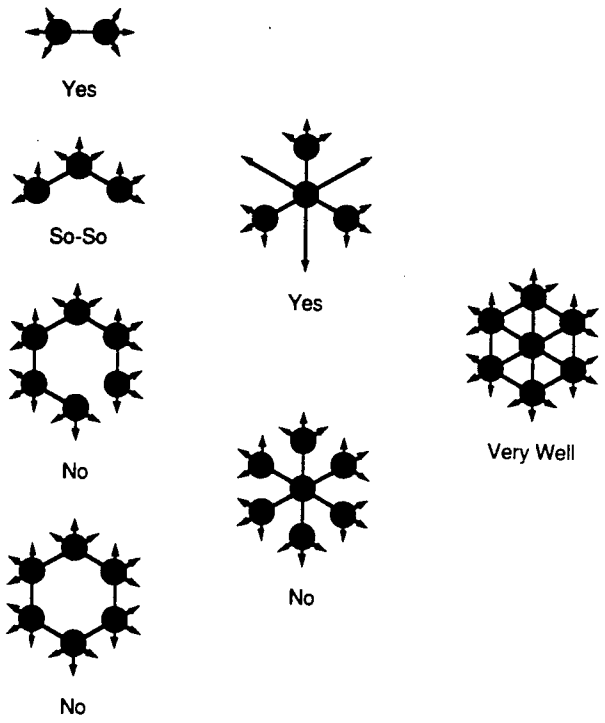

FIG. 14. Qualitative summary of geometries that support phase locking.

The second approach is to create an array of modules. If the microwave pulse length could be extended, so that it was long compared to the propagation time between modules, the array would be the analogue to the present module, with modules replacing the individual magnetrons in the present picture. If the pulse length cannot be extended sufficiently, the modules could not interact as peers. Instead, one module would have to be master to the rest. A successful test of this interaction would be a proof-of-principle demonstration that could lead to a system with an unlimited amount of rf power.

ACKNOWLEDGMENTS

The authors would like to acknowledge the technical assistance of R. Courtney and S. Montalvo and programming of the data acquisition system by E. Willis. This work was supported by SDIO/IS&T, managed by the Harry Diamond Laboratories, and DNA.

[1] J. G. Small, W. O. Eckhardt, and F. Chilton, Proc. SPIE **1061**, 342 (1989).
[2] D. Price and H. M. Sze, IEEE Trans. Plasma Sci. **18**, 580 (1990).
[3] R. Adler, Proc IRE **34**, 351 (1946).
[4] J. Benford, H. Sze, W. Woo, R. R. Smith, and B. Harteneck, Phys. Rev. Lett. **62**, 969 (1989).
[5] D. Price, H. Sze, and D. Fittinghoff, J. Appl. Phys. **65**, 5185 (1989).
[6] H. Sze, D. Price, and B. Harteneck, J. Appl. Phys. **67**, 2278 (1990).
[7] H. Sze, D. Price, B. Harteneck, and N. Cooksey, J. Appl. Phys. **68**, 3073 (1990).
[8] K. J. Hendriks, R. Adler, and R. C. Noggle, J. Appl. Phys. **68**, 820 (1990).
[9] W. Woo, J. Benford, D. Fittinghoff, B. Harteneck, D. Price, R. Smith, and H. Sze, J. Appl. Phys. **65**, 861 (1989).
[10] B. van der Pol, Philos. Mag. **7**, 65 (1927).
[11] A. Palevsky and G. Bekefi, Phys. Fluids **22**, 986 (1979).
[12] R. R. Smith, H. Sze, B. Harteneck, and J. Benford, IEEE Trans. Plasma Sci. **16**, 234 (1988).

APPENDIX C

POWER BEAMING REPORT

Earth to Satellite Microwave Power Transmission for SDI Applications

New York University
Department of Applied Science
Dr. Gabriel Miller, Principal Investigator
Seth Potter, Graduate Assistant

Submitted to Physics International
San Leandro, California
August 21, 1991

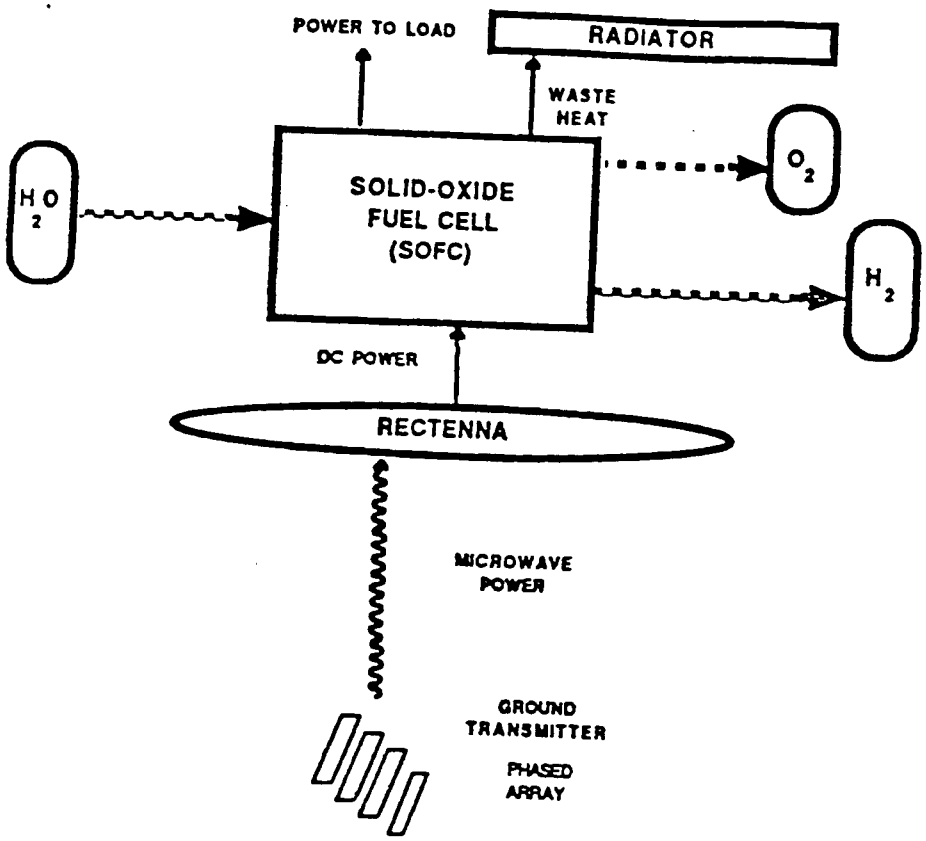

Figure 1. Energy conversion steps in the MTL (Microwave to Low Earth Orbit) system. Microwave power is beamed to the platform and is converted to chemical energy by use of a fuel cell and recovered for use as needed. (From Reference 13.)

SYSTEMS CONCEPT

The first step in the energy conversion scheme is the generation of DC electrical power at ground based stations, and conversion to RF (microwave) frequencies using microwave generators. The choice of the microwave generators and the transmitting antennas for power transmission using microwave beams have been dealt with independently in Refs. 1, 2, 9, 10, 11, and 12. Magnetrons, klystrons, solid state devices and travelling wave tubes (TWT's) are among some of the microwave generators [1,2,10] considered in past power beaming research. The SDI applications considered here will probably use relativistic klystrons. Many innovative concepts have been suggested for the design of the transmitting antenna including circular dish antennas, slotted phased arrays[1], and arrays of parabolic antennas with Cassegrain feed. Wood[11], has proposed a large antenna of a flat geometry, consisting of many identical reflecting panels moved by linear actuators to generate and power the SHARP (Stationary High Altitude Platform), which is essentially a microwave powered remote controlled aircraft.

The CO-OPS (Carbon Dioxide Observational Platform) study[9,10] essentially considered three arrays -- dish, slotted array, and slotted arrays on pedestal, and concluded that the

prime candidate for the ground power system is the slotted arrays on pedestal. An important feature which emerges from the CO-OP's study, which was treated at some length by us earlier[1,2], and of relevance to any beamed microwave concept, is the power control, steering and focussing of the microwave beam. Fig 2, adapted from the CO-OP's study[9] describes the ground power system and associated controls. Power control is necessary as excess power is likely to overheat the diodes and can reduce the life of the rectenna, and in some cases even destroy the diodes[12] in the rectenna. The beam steering and focussing are achieved by either a central or a distributed system[9]. In the central system the azimuth and elevation of the platform is measured, the appropriate steer and focus are calculated and phase control is provided over the aperture. In the distributed system to be used here, however, the phase gradients are measured and power control is achieved by a feedback system between the platform and the ground station.

The next step in the energy conversion scheme is the reception and rectification of the power by the rectenna onboard the MTL system. The rectenna technology has been dealt with at length in our earlier papers[1,2]. The rectenna is deployed similar to the thermal radiators - essentially as a parasol on a spin stabilized boom. Such a deployment has its advantages in that the rectenna can be spun out in order to deploy it initially, the orientation of the boom can be controlled with respect to the earth and further the polarization losses in the rectenna can be controlled. However power conditioning from the rectenna to the fuel cell is very important, for as shown in Figure 3, the power received at the rectenna varies approximately as a gaussian during the beaming, whereas the input to the electrolyzer (which is essentially the fuel cell operating in the reverse or regenerative mode) has to be approximately at steady voltage. The PC / C (Power Conditioning and Control) is achieved by a dynamic switching circuit, shown in Figure 4.

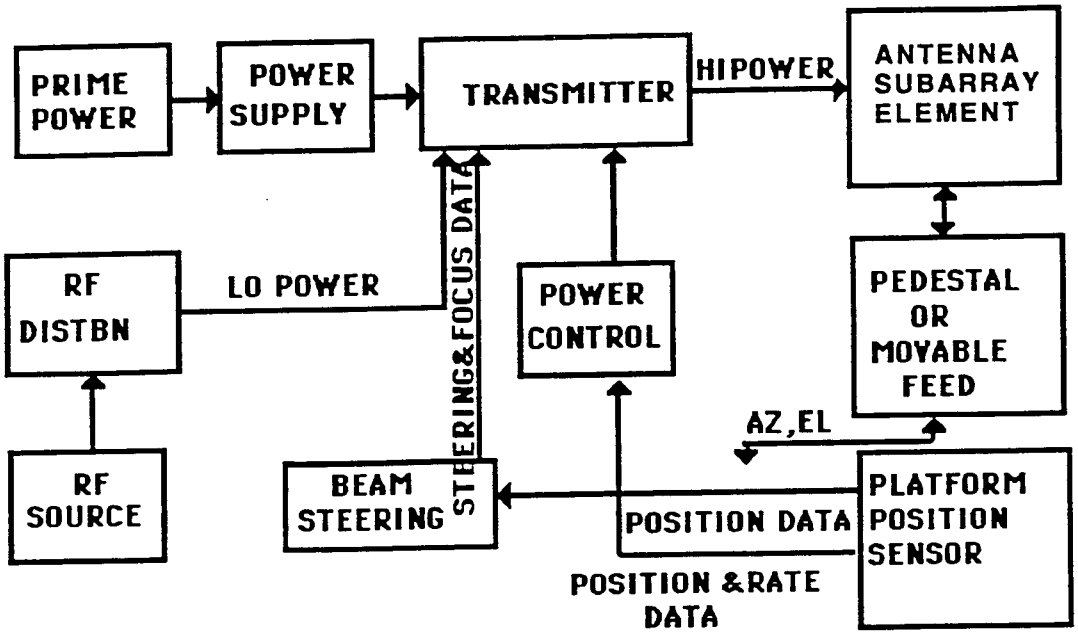

Figure 2. Block diagram of the ground microwave power system which illustrates the power control, beam steering and focussing adapted from the CO-OPS study performed by Lockheed. (Reference 9.)

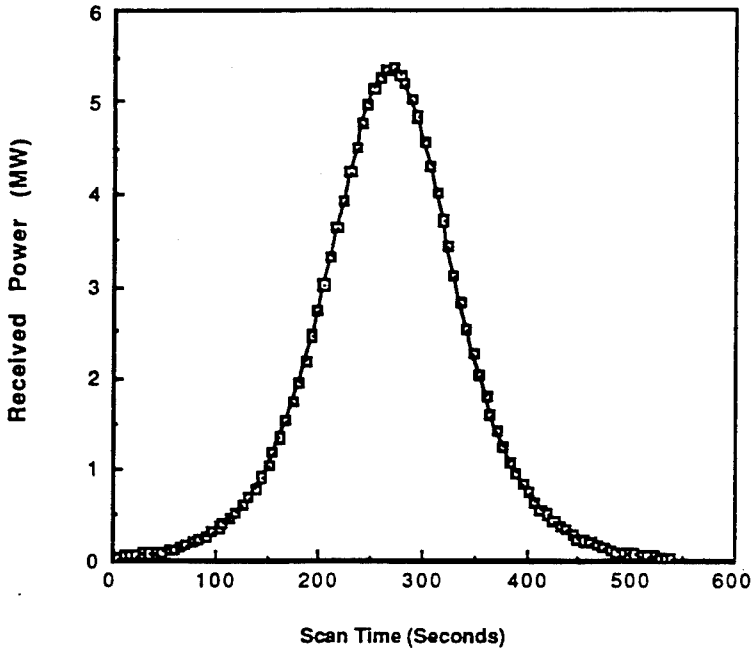

Figure 3. Variation of received power on the face of the rectenna and with scan time (fraction of the orbit during which beaming occurs) for an 800 Km altitude platform, and a ratio of rectenna to transmitter size of 62/500. (From Reference 13.)

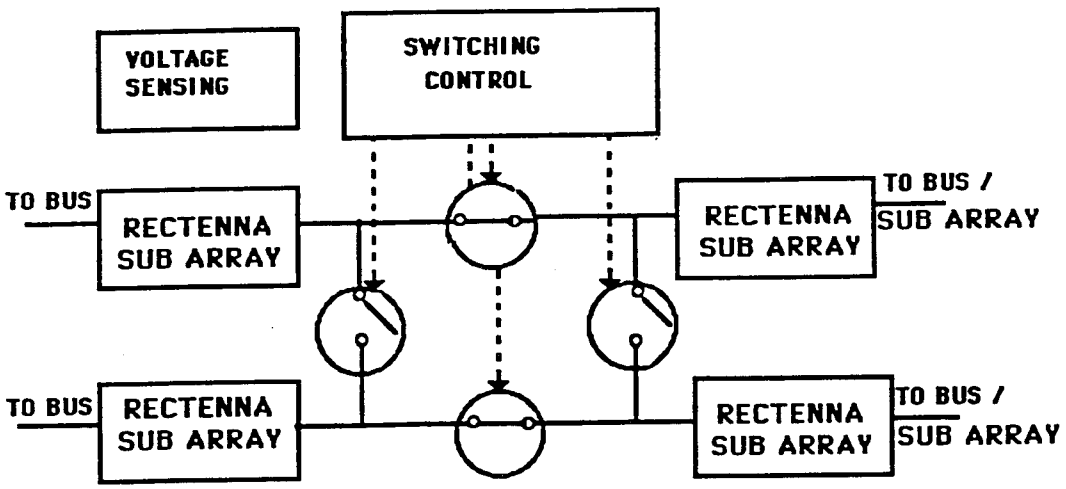

Figure 4. Block diagram of the power conditioning from the rectenna to the fuel cell using a dynamic solid state switching circuit to change the combination of the sub arrays from series to parallel as the platform is energized during beaming. (From Reference 13.)

The rectenna is divided into a number of sub arrays which can be coupled together in required series-parallel combinations, which produce the required output. However some other components will also be necessary to complete the power conditioning, which will include voltage and current limiters, since the rectenna feeds the bus as well as the electrolyzer during beaming.

ANALYSIS OF THE MTL SYSTEM

In order to assess the feasibility of Earth to satellite microwave power transmission for SDI satellites, two computer programs were used. The first was an orbit program which tracks satellites as they pass over a ground station. Satellites in polar orbit at 200, 300, and 400 kilometer altitudes were tracked as they passed over a ground station located at 65° North latitude. The program computes the azimuth and elevation of the satellite as a function of time. The second computer program uses this data to compute rectenna size for a given transmitted power, housekeeping power, frequency, and transmitter size. Peak beam intensity at the rectenna is also computed. It was assumed that the number of ground stations and their longitude is such that each satellite passes over a ground station once per orbit. The scan times used are the amount of time that a given satellite is at least 15° over the horizon as it passes over a given ground station. The scan times per orbit are given in Table 1. This table also shows orbital period and f (the fraction of the orbit during which power transmission takes place; it is found by dividing scan time per orbit by orbital period). In order to obtain a consistent set of data, the rectenna sizes were initially computed for a microwave frequency of 2.45 GHz (wavelength = 12.25 cm) and a transmitter diameter of 500 meters. The effect of increasing the frequency was then examined.

In order to size the rectenna and other related subsystems the second computer program, mentioned above, was developed, based on the analysis developed earlier[1,2]. This program computes the average reception efficiency $\langle\eta_r\rangle$, rectenna size D_r and peak beam intensity I_o on the rectenna plane for a given housekeeping power level P_H, altitude h and transmitted power level P_t. The required average efficiency, in order to size the rectenna for a given housekeeping power level and transmitted power level, is determined from an energy conservation criterion on the platform. For conservation of energy,

$$P_H (T - f T) + P_H f T = P_t f T \langle\eta_r\rangle \eta_s \quad (1)$$

which can be solved for the required average reception efficiency,

$$\langle\eta_r\rangle = P_H / (P_t f \eta_s) \quad (2)$$

ywhere T is the orbital time period, f T is the transmission time during which energy is beamed to the platform, f is the accessibility fraction mentioned above, and η_s is the systems efficiency. The parameter η_s includes the rectenna conversion efficiency of microwave to DC, the power conditioning efficiency, and the "round trip" efficiency of the fuel cell (i.e, in both the electrolyzer and cell modes). The value of η_s is held fixed at 0.70. The rectenna diameter is fixed at a certain value and the transmission efficiency $\langle\eta_r\rangle$ is computed using equations given based on orbital geometry[1,2]. The calculated efficiency is compared with the required efficiency computed from Equation 2, and the rectenna size is either increased or decreased iteratively until the energy conservation criterion is fulfilled. This computation is repeated for different transmitted and housekeeping power levels and altitudes. Once the size of the rectenna is fixed, the average efficiency is calculated, and the peak beam intensity is determined from:

$$I_o = \frac{P_t}{\pi}\left\{\frac{2 D_t \cos\theta_o \cos\theta_{xo} \cos\theta_{yo}}{\lambda h}\right\}^2 \quad (3)$$

Tables 2A through 4B show the results from the microwave transmission program. The contract required that we assess microwave power transmission for both low (100 kilowatts) and high (1 megawatt) levels of onboard housekeeping power (P_H). Levels of transmitted power (P_t) appropriate for these levels of housekeeping power were chosen. Due to the nature of the program, it was easy to assess two levels of housekeeping power for a given transmitted power. Thus, the tables for 100 kW of housekeeping power also include 200 kW of housekeeping power. The tables for 1 MW of housekeeping power also include 500 kW of housekeeping power. This provides insight into how rectenna diameter scales with housekeeping power if all other quantities are held constant. Note in the tables that for a given P_t, doubling P_H doubles $\langle\eta_r\rangle$, as expected from Equation 2 (the doubling of $\langle\eta_r\rangle$ is not precise, since the program only computes rectenna diameter to the nearest meter). The rectenna area increases, and in fact more than doubles (that is, the rectenna diameter increases by a factor of more than $\sqrt{2}$), since the beam intensity is not constant across the rectenna. The peak beam intensity stays the same, since the rectenna is intercepting a greater portion of the same beam for higher P_H.

Since the two high housekeeping powers used (500 and 1000 kW) were five times the values of the two low housekeeping powers used (100 and 200 kW), values of transmitted power used in the former cases were five times the latter. One exception to this is that an extra P_t case (50 MW) was used for low P_H. Since 50 MW of P_t was used for high P_H, the scaling of rectenna with P_H is shown. From Equation 2, it is seen that at a given scan fraction f (i.e., at a given altitude), $\langle\eta_r\rangle$ depends on the ratio P_H / P_t. Thus, at a given altitude, rectenna diameter will depend on this ratio, and not on the specific values of P_H and Pt. Hence, the rectenna diameters and the values of $\langle\eta_r\rangle$ in a given "A" table (low housekeeping powers) will match those in the corresponding "B" table (high

housekeeping powers). However, the peak beam intensity will increase and will vary directly with P_t.

In designing SDI satellites, rectenna size must be kept to a minimum in order to minimize target area, atmospheric drag, and launch costs. As Tables 2A through 4B indicate, one way of achieving this is by using high levels of transmitted power. This results in low values of $<\eta_r>$; hence, much of the transmitted power goes to waste. Furthermore, the peak beam intensities may increase to levels that are beyond those which the rectenna can handle. Such intensities may cause direct heating of the rectenna, and, more importantly, an overload of the diodes in the rectenna. Current designs for 2.45 GHz rectennas can handle 250 to 300 W / m^2 in space. Rectennas designed for 2.45 GHz have 200 diodes per square meter; this corresponds to about 1.5 watts per diode. Diodes for use in rectennas have been successfully tested at 20 watts each if convective cooling is used; this corresponds to 4000 W / m^2. However, our results show peak beam intensities in the tens of thousands of watts per square meter for higher levels of transmitted power. The highest intensity shown in the tables is approximately 78,700 W / m^2 (see Table 2B). This corresponds to nearly 400 watts per diode. Thus, the rectennas used in such cases will require thermal redesign, employing special coatings and passive cooling heat sinks. In addition, more advanced diodes may have to be developed.

An alternate method of minimizing rectenna size is to use relatively small levels of transmitted power, but to increase the frequency of the microwave beam. The rectenna diameter is directly proportional to wavelength (that is, inversely proportional to frequency). The peak beam intensity is inversely proportional to the area occupied by the main lobe, and is thus inversely proportional to the square of the wavelength (that is, directly proportional to the square of the frequency). If the frequency increases by x, then the rectenna diameter decreases by 1/x, and the peak beam intensity increases by x^2. Although it may seem that this offers no thermal advantage over an x^2 increase in transmitted power at the original frequency (which would also allow for a smaller rectenna), it must be kept in mind that the number of diodes per square meter of rectenna will also increase by x^2; the total number of diodes in the rectenna will thus stay the same. This is because each rectenna element has one diode, and the size and spacing of the elements is proportional to wavelength. Thus, for a given level of transmitted power, as the frequency is increased, the rectenna size will decrease, but the power in each diode will remain the same. From Equation 2, and from Tables 2A through 4B, it is seen that the largest values of rectenna diameter and $<\eta_r>$ occur at the largest values of the ratio P_H / P_t; specifically, 1/50 in the cases examined. It is seen, especially for the 200 kilometer orbit, that for such power ratios, the rectennas are impractically large and the values of $<\eta_r>$ are near 100%. (This shows that values of P_H / P_t much larger than about 1/50 are not practical.) Tables 5, 6, and 7 show the effect of frequency on the size of the rectennas for $P_H / P_t = 1/50$. At a given altitude, for a given value of P_H / P_t, the value of $<\eta_r>$ does not change with frequency. The new frequencies considered are 5.9, 35, and 94 GHz.

Increasing the frequency may be a promising means by which the rectenna size can be minimized without overloading the diodes. For example, suppose a housekeeping power of 1 MW is needed at an altitude of 300 kilometers. A transmitted power level of 50 MW can be used. This results in a fairly high value of $<\eta_r>$ (about 64%), but the rectenna is an unwieldy 366 meters across (Table 3B) if we use the 2.45 GHz frequency. If we wish to downsize the rectenna to roughly 150 meters, we are faced with two alternatives. We can increase the power transmitted to 75 MW, but the maximum power handled per diode goes from 59 W / m^2 (11,726 watts per square meter / 200 diodes per square meter) to 88 W / m^2 (17,589 watts per square meter / 200 diodes per square meter; see Table 3B). In addition, $<\eta_r>$ decreases to approximately 42%, so that more of the transmitted power is wasted. Alternatively, we can maintain a transmitted power level of 50 MW, and increase

the frequency to 5.9 GHz. This results in a rectenna diameter of 152 meters, while preserving a power handled per diode of 59 watts and an $<\eta_r>$ of 64% (see Table 6). By increasing the frequency to 35 GHz, a rectenna only 26 meters across becomes possible, while maintaining the same power handled per diode and $<\eta_r>$. However, there will now be a peak beam intensity of approximately 2.4 MW / m^2 incident on the rectenna; the thermal effects of such an intense beam on the rectenna must be examined.

The size of the rectenna can be decreased if the diameter of the transmitter array is increased. An increase in transmitter diameter by a factor of x will allow a decrease in the rectenna diameter by the same factor. However, both the peak beam intensity and the power per diode will increase by a factor of x^2. (Since the wavelength is being held constant in this case, the number of diodes per square meter remains fixed.)

TABLE 1
ORBITAL PERIODS AND SCAN TIMES

Altitude (km)	Period (min)	Period (sec)	Scan Time (sec)	Scan Fraction (f)
200	88.44	5306	168	0.0317
300	90.46	5428	240	0.0442
400	92.50	5550	300	0.0541

TABLE 2A
200 KILOMETER ORBIT, LOW HOUSEKEEPING POWER

P_t (MW)	P_H (kW)	Rectenna Diameter (meters)	Peak Beam Intensity (W / m^2)	$\langle \eta_r \rangle$ (%)
10	100	108	5247	44.20
10	200	1008	5247	89.25
15	100	65	7870	29.52
15	200	204	7870	59.18
20	100	50	10,493	21.66
20	200	108	10,493	44.20
25	100	43	13,117	17.58
25	200	79	13,117	35.46
30	100	38	15,740	14.59
30	200	65	15,740	29.52
50	100	27	26,233	8.27
50	200	43	26,233	17.58

TABLE 2B
200 KILOMETER ORBIT, HIGH HOUSEKEEPING POWER

P_t (MW)	P_H (kW)	Rectenna Diameter (meters)	Peak Beam Intensity (W / m^2)	$\langle \eta_r \rangle$ (%)
50	500	108	26,233	44.20
50	1000	1008	26,233	89.25
75	500	65	39,350	29.52
75	1000	204	39,350	59.18
100	500	50	52,466	21.66
100	1000	108	52,466	44.20
125	500	43	65,583	17.58
125	1000	79	65,583	35.46
150	500	38	78,699	14.59
150	1000	65	78,699	29.52

TABLE 3A
300 KILOMETER ORBIT, LOW HOUSEKEEPING POWER

P_t (MW)	P_H (kW)	Rectenna Diameter (meters)	Peak Beam Intensity (W / m^2)	$\langle \eta_r \rangle$ (%)
10	100	101	2345	31.35
10	200	366	2345	63.66
15	100	71	3518	20.66
15	200	145	3518	42.10
20	100	58	4690	15.40
20	200	101	4690	31.35
25	100	50	5863	12.16
25	200	82	5863	24.89
30	100	44	7035	9.81
30	200	71	7035	20.66
50	100	32	11,726	5.56
50	200	50	11,726	12.16

TABLE 3B
300 KILOMETER ORBIT, HIGH HOUSEKEEPING POWER

P_t (MW)	P_H (kW)	Rectenna Diameter (meters)	Peak Beam Intensity (W / m^2)	$\langle \eta_r \rangle$ (%)
50	500	101	11,726	31.35
50	1000	366	11,726	63.66
75	500	71	17,589	20.66
75	1000	145	17,589	42.10
100	500	58	23,452	15.40
100	1000	101	23,452	31.35
125	500	50	29,314	12.16
125	1000	82	29,314	24.89
150	500	44	35,177	9.81
150	1000	71	35,177	20.66

TABLE 4A
400 KILOMETER ORBIT, LOW HOUSEKEEPING POWER

P_t (MW)	P_H (kW)	Rectenna Diameter (meters)	Peak Beam Intensity (W / m^2)	$\langle\eta_r\rangle$ (%)
10	100	107	1322	25.49
10	200	260	1322	51.88
15	100	79	1983	16.75
15	200	141	1983	34.42
20	100	65	2643	12.29
20	200	107	2643	25.49
25	100	57	3304	9.84
25	200	90	3304	20.27
30	100	50	3965	7.82
30	200	79	3965	16.75
50	100	37	6609	4.50
50	200	57	6609	9.84

TABLE 4B
400 KILOMETER ORBIT, HIGH HOUSEKEEPING POWER

P_t (MW)	P_H (kW)	Rectenna Diameter (meters)	Peak Beam Intensity (W / m^2)	$\langle\eta_r\rangle$ (%)
50	500	107	6609	25.49
50	1000	260	6609	51.88
75	500	79	9913	16.75
75	1000	141	9913	34.42
100	500	65	13,217	12.29
100	1000	107	13,217	25.49
125	500	57	16,522	9.84
125	1000	90	16,522	20.27
150	500	50	19,826	7.82
150	1000	79	19,826	16.75

TABLE 5
VARIATION OF RECTENNA DIAMETER WITH FREQUENCY
FOR 200 KILOMETER ORBIT WITH P_H / P_t =1/50
($\langle\eta_r\rangle$ = 89.25 %)

Frequency (GHz)	Rectenna Diameter (meters)	Peak Beam Intensity (W / m^2) Low power)*	Peak Beam Intensity(W / m^2) (High power)**
2.45	1008	5247	26,233
5.9	419	30,430	152,100
35.0	71	1.071×10^6	5.354×10^6
94.0	26	7.724×10^6	38.62×10^6

*P_t = 10 MW, P_H = 200 kW, power per diode = 26 watts.
**P_t = 50 MW, P_H = 1000 kW, power per diode = 131 watts.

TABLE 6
VARIATION OF RECTENNA DIAMETER WITH FREQUENCY
FOR 300 KILOMETER ORBIT WITH P_H / P_t =1/50
($\langle\eta_r\rangle$ = 63.66 %)

Frequency (GHz)	Rectenna Diameter (meters)	Peak Beam Intensity (W / m^2) (Low power)*	Peak Beam Intensity (W / m^2) (High power)**
2.45	366	2345	11,726
5.9	152	13,600	68,000
35.0	26	478,600	2.393×10^6
94.0	9.5	3.452×10^6	17.26×10^6

*P_t = 10 MW, P_H = 200 kW, power per diode = 12 watts.
**P_t = 50 MW, P_H = 1000 kW, power per diode = 59 watts.

TABLE 7
VARIATION OF RECTENNA DIAMETER WITH FREQUENCY
FOR 400 KILOMETER ORBIT WITH P_H / P_t =1/50
($\langle\eta_r\rangle$ = 51.88 %)

Frequency (GHz)	Rectenna Diameter (meters)	Peak Beam Intensity (W / m^2) (Low power)*	Peak Beam Intensity (W / m^2) (High power)**
2.45	260	1322	6609
5.9	108	7667	38,330
35.0	18	269,800	1.349×10^6
94.0	6.8	1.946×10^6	9.729×10^6

*P_t = 10 MW, P_H = 200 kW, power per diode = 6.6 watts.
**P_t = 50 MW, P_H = 1000 kW, power per diode = 33 watts.

CONCLUSIONS

A study of the MTL (Microwave to Low Earth Orbit) concept to power SDI missions has been made. The size of the rectennas and the average reception efficiencies needed for four levels of housekeeping power (100, 200, 500, and 1000 kW) has been computed for satellites in polar orbit at altitudes of 200, 300, and 400 kilometers. The design of the MTL system for a given altitude and level of housekeeping power involves a compromise between rectenna size, transmitter array size, level of transmitted power, and frequency. The need to keep rectennas small, and the need to avoid overloading the rectenna diodes are the major constraints on the system.

REFERENCES

1) Hoffert, M.I., et. al., "Earth to Satellite Microwave Beams: Innovative Approach to Space Power," Microwave and Particle Beam Sources and Propagation, Norman Rostoker, Editor, Proc. SPIE Vol. 873. pages 148-169.(1988).
2) Hoffert, M.I., et. al., "Earth to Satellite Microwave Power Transmission," Journal of Propulsion and Power, 1989.
3) Carroll, W. P., Personal Communication, Nov 1988.
4) Sholtis, J.A. (1987) "Programmatic, Technical, and Safety Overview of the SP-100 Space Reactor Power Program," Presented at the 3rd SDI Workshop on Space Experimentation, Orlando, Florida, June 2-4, 1987; available from SP-100 Program Office, Air Force Element, Dept. of Energy, DEP/NE-521 (GTN), Washington, DC.
5) Space Power Architecture Study Report. Vol 6, USAF Space Technology Center, Kirtland AFB, NM.
6) Luoma, J. R., "U.S. Turning to New Technologies to Clean up Arms Plants," New York Times, Jan 3, 1989, p C4.
7) Broad, W J., "New Plans for Space Reactors Raise Fears of Nuclear Debris," New York Times, October 18, 1988, p C1.
8) Brune, J., "Powering SDI," New York Newsday Jan 3, 1989, part III, p 1.
9) Carbon Dioxide Observational Platform System Study (CO-OPS) Technical Review, Prepared for NASA / George C. Marshall Space Flight Center by Lockheed - Georgia Company.Feb 1986.
10) Stephens, J.B., and Thompson, W.E., "System Study of the Carbon Dioxide Observational Platform Study (CO-OPS)," NASA Technical Paper 2696. March 1987.
11) Wood, P.J., "A Concept for A Large Steerable Antenna Using Individually Displaced Panels," Paper presented at the IEEE Montech Conference on Antennas and Communications, Sept. 29 - Oct. 1, 1986, Montreal, Canada.
12) Brown, W.C., "Earth to Space DC to DC Power Transmission System Utilizing a Microwave Beam as a Source of Energy for Electric Propelled Interorbital Vehicles," Presented at AIAA Electric Propulsion Conference, Sept. 30 - Oct. 2, 1985, Alexandria, VA.
13) Kadiramangalam, M.N., Hoffert, M.I., and Miller, G., "Onboard Energy Conversion and Thermal Analysis of the MTL System," Microwave and Particle Beam Sources and Directed Energy Concepts, Howard E. Brandt, editor, Proc. SPIE, Vol. 1061, pages 313 - 341 (1989).

DISTRIBUTION LIST

DNA-TR-94-49

DEPARTMENT OF DEFENSE

BALLISTIC MISSILE DEFENSE ORGANIZATION
ATTN: T/SL

DEFENSE INFORMATION SYSTEMS AGENCY
ATTN: COMMANDER

DEFENSE INTELLIGENCE AGENCY
ATTN: DT-4A W E THOMPSON
ATTN: DT-4C DR J COLEMAN
ATTN: PGI-4

DEFENSE NUCLEAR AGENCY
ATTN: DFRA JOAN MA PIERRE
2 CY ATTN: IMTS
ATTN: OPNA
ATTN: RAEM K SCHWARTZ
ATTN: RAES
ATTN: RAST
ATTN: RAST W SUMMA

DEFENSE TECHNICAL INFORMATION CENTER
2 CY ATTN: DTIC/OC

FIELD COMMAND DEFENSE NUCLEAR AGENCY
ATTN: FCTO
ATTN: FCTT DR BALADI

NATIONAL DEFENSE UNIVERSITY
ATTN: NWCO

NATIONAL SECURITY AGENCY
ATTN: TECHNICAL LIBRARY

NET ASSESSMENT
ATTN: DOCUMENT CONTROL

DEPARTMENT OF THE ARMY

ADVANCED RESEARCH PROJECT AGENCY
ATTN: DED

ARMY RESEARCH LABORATORIES
ATTN: TECH LIB
ATTN: AMSRL-WT-NA
ATTN: AMSRL-WT-NF LOU JASPER JR
ATTN: AMSRL-WT-NH G MERKEL
ATTN: SLCHD-NW-RH R GILBERT

DEP CH OF STAFF FOR OPS & PLANS
ATTN: DAMO-ODW

PED MISSILE DEFENSE SFAE-MD-TSD
ATTN: CSSD-SL

U S ARMY ATMOSPHERIC SCIENCES LAB
ATTN: SLCAS-AS

U S ARMY COMM R&D COMMAND DEFENSE CMD
ATTN: CSSD-SA-E

U S ARMY ENGINEER DIV HUNTSVILLE
ATTN: HNDED-SY

U S ARMY NATIONAL GROUND INTELLIGENCE CTR
ATTN: IAFSTC-RMT

U S ARMY NUCLEAR & CHEMICAL AGENCY
ATTN: MONA-NU DR D BASH

U S ARMY RESEARCH LAB
ATTN: SLCBR-SS-T
ATTN: SLCBR-VL
ATTN: SLCBR-VL-LD

U S ARMY TEST & EVALUATION COMMAND
ATTN: TECHNICAL LIBRARY SI-F

U S ARMY VULNERABILITY ASSESSMENT LAB
ATTN: SLCVA-TAC R FLORES

U S ARMY WAR COLLEGE
ATTN: LIBRARY

US ARMY MATERIEL SYS ANALYSIS ACTVY
ATTN: AMXSY-CR

DEPARTMENT OF THE NAVY

DEPARTMENT OF THE NAVY
ATTN: CODE R41
ATTN: CODE 425

NAVAL RESEARCH LABORATORY
ATTN: CODE 4650 T WIETING
ATTN: CODE 4740 W MANNHEIMER
ATTN: CODE 5227 RESEARCH REPORT
ATTN: CODE 8320.1 V FOLEN

NAVAL SURFACE WARFARE CENTER
ATTN: CODE H-21
ATTN: R RICHARDSON

NAVAL TECHNICAL INTELLIGENCE CTR
ATTN: DEOO
ATTN: LIBRARY

OFFICE OF CHIEF NAVAL OPERATIONS
ATTN: NOP 098
ATTN: NOP 551
ATTN: NOP 941F
ATTN: NOP-956
ATTN: NUC AFFAIRS & INT'L NEGOT BR
ATTN: N88OE

PROGRAM EXECUTIVE OFFICE
ATTN: AIR 5161
ATTN: AIR-5164
ATTN: AIR-933

SPACE & NAVAL WARFARE SYSTEMS CMD
ATTN: PMW-145
ATTN: TECHNICAL LIBRARY

THEATER NUCLEAR WARFARE PROGRAM OFC
ATTN: PMS 423 CDR DOOLING

DEPARTMENT OF THE AIR FORCE

AFIWC/MSO
ATTN: TECHNICAL LIBRARY

AIR FORCE CTR FOR STUDIES & ANALYSIS
ATTN: AFSAA/SAI

AIR UNIVERSITY LIBRARY
ATTN: AUL-LSE

PHILLIPS LABORATORY
ATTN: B SINGARAJU

SPACE DIVISION/IN
ATTN: IND

USAF ROME LABORATORY TECHNICAL LIBRARY FL2810
ATTN: RBCM
ATTN: RBCT

DEPARTMENT OF ENERGY

LAWRENCE LIVERMORE NATIONAL LAB
ATTN: H CABAYAN

LOS ALAMOS NATIONAL LABORATORY
ATTN: MICHAEL V FAZIO
ATTN: MS A112 M GILLESPIE
ATTN: MS D408
ATTN: MS F617
ATTN: LT COL J DUNN
ATTN: MS H827
ATTN: REPORT LIBRARY

SANDIA NATIONAL LABORATORIES
ATTN: DEPT 1235 J HOFFMAN
ATTN: DEPT 7555
ATTN: ORG 9300 RICH WESTFALL
ATTN: TECH LIB 3141

U S DEPT OF ENERGY IE-24
ATTN: J BUSSE

OTHER GOVERNMENT

CENTRAL INTELLIGENCE AGENCY
ATTN: OSWR/NED 5S09 NHB
ATTN: OSWR/SSD/SWB
ATTN: OSWR/STD/TTB

FEDERAL EMERGENCY MANAGEMENT AGENCY
ATTN: SL-CD-MP

DEPARTMENT OF DEFENSE CONTRACTORS

ALLIED-SIGNAL, INC
ATTN: DOCUMENT CONTROL

BATTELLE MEMORIAL INSTITUTE
ATTN: V PUGLIELLI

BDM FEDERAL INC
ATTN: E DORCHAK

BDM FEDERAL INC
ATTN: LIBRARY

BOEING CO
ATTN: D EGELKROUT

BOOZ ALLEN & HAMILTON INC
ATTN: L ALBRIGHT

BOOZ-ALLEN & HAMILTON, INC
ATTN: TECHNICAL LIBRARY

CHARLES STARK DRAPER LAB, INC
ATTN: LIBRARY

E-SYSTEMS, INC
ATTN: TECH INFO CTR

EG&G MANAGEMENT SYSTEMS, INC
ATTN: J GILES

HONEYWELL SYSTEMS & RESEARCH CENTER
ATTN: T CLARKIN

INSTITUTE FOR DEFENSE ANALYSES
ATTN: CLASSIFIED LIBRARY
ATTN: TECH INFO SERVICES

JAYCOR
ATTN: CYRUS P KNOWLES
ATTN: E WENAAS
ATTN: M SCHULTZ JR

JAYCOR
ATTN: R DUBOIS

KAMAN SCIENCES CORP
ATTN: C EKLUND

KAMAN SCIENCES CORP
ATTN: DASIAC

KAMAN SCIENCES CORPORATION
ATTN: DASIAC
ATTN: R RUTHERFORD

LOCKHEED MISSILES & SPACE CO, INC
ATTN: G LUM ORG 81-63
ATTN: TECH INFO CTR

LOCKHEED SANDERS, INC
ATTN: BRIAN G CARRIGG

LOGICON R & D ASSOCIATES
ATTN: E QUINN

LOGICON R & D ASSOCIATES
ATTN: J P CASTILLO
ATTN: R PARKER

LORAL VOUTHG SYSTEMS CORP
2 CY ATTN: LIBRARY

MARTIN MARIETTA
ATTN: P HEILAND

MISSION RESEARCH CORP
ATTN: EMP GROUP

MISSION RESEARCH CORP
ATTN: D SULLIVAN

MISSION RESEARCH CORP
ATTN: M BOLLEN

MISSION RESEARCH CORP
ATTN: J LUBELL
ATTN: J R CURRY

MITRE CORPORATION
ATTN: CORPORATE INFO SVCS
ATTN: M FITZGERALD

PACIFIC-SIERRA RESEARCH CORP
ATTN: H BRODE

PHOTOMETRICS, INC
ATTN: I L KOFSKY

PHYSICS INTERNATIONAL CO
ATTN: B HARTENECK
ATTN: D V DRURY
ATTN: G MILLER
ATTN: J BENFORD
ATTN: J S LEVINE
ATTN: L SMITH
ATTN: L THOMPSON
ATTN: N AIELLO
ATTN: N J COOKSEY
ATTN: P SINCERNY
ATTN: R R SMITH
ATTN: S ASHBY
ATTN: S POTTER

PULSE SCIENCES, INC
ATTN: TECHNICAL LIBRARY

RESEARCH TRIANGLE INSTITUTE
ATTN: M SIMONS

SCIENCE APPLICATIONS INTL CORP
ATTN: W CHADSEY

SRI INTERNATIONAL
ATTN: ELECTROMAG SCI LAB

TRW INC
ATTN: LIBRARIAN

TRW INC
ATTN: TIC

TRW SPACE & DEFENSE SECTOR
ATTN: D M LAYTON
ATTN: A SPEHAR

UNISYS CORPORATION-DEFENSE SYSTEMS
ATTN: TECHNICAL LIBRARY

UNITED TECHNOLOGIES CORP
ATTN: R D TOTTON

VARIAN ASSOCIATES INC
ATTN: TECHNICAL LIBRARY